Prediction of the Elastic Strain Limit of Tendons

Alejandra Magaly Reyes Lúa

Master of Science Thesis

TU Delft Delft University of Technology

Biomedical Engineering

Prediction of the Elastic Strain Limit of Tendons

Master of Science Thesis

For obtaining the degree of Master of Science in Biomedical Engineering at Delft University of Technology

Alejandra Magaly Reyes Lúa

November 22, 2012

Faculty of Mechanical, Maritime and Materials Engineering · Delft University of Technology

Delft University of Technology
Department of Biomedical Engineering

The undersigned hereby certify that they have read and recommend to the Faculty of Mechanical, Maritime and Materials Engineering for acceptance a thesis entitled

Prediction of the Elastic Strain Limit of Tendons

by

Alejandra Magaly Reyes Lúa

in partial fulfillment of the requirements for the degree of

Master of Science.

Dated: November 22, 2012

Supervisor(s):

Prof.Dr.Ir. H.H. Weinans

Dr. A.A. Zadpoor

Reader(s):

Dr.Ir. M. Janssen

Acknowledgements

I would like to thank to Consejo Nacional de Ciencia y TecnologÃŋa (CONACYT) for the support they gave me to finance my master studies in this university, which otherwise would have not been possible.

I would like to make a special recognition to Deepesh who gave me moral support from beginning to end and shared nice discussions with me about the topic, resulting in fruitful contributions to the project. I would also like to thank my friends Martina Cuschieri and Mahshid Vashaghian who were there for me in the most difficult moments and helped me go through them successfully.

My family was a key aspect of my ongoing drive to achieve goals and I thank them for their unbreakable trust on me. Last but not the least is the acknowledgment to my supervisors Prof. Dr. Ir. Harrie Weinans, Dr. Amir Zadpoor and Dr. Holger Jahr who gave insightful suggestions for the progress of the project.

ABSTRACT

The elastic strain limit of the tendon appears to be an omnipresent parameter in the literature in many of the problems described related to its pathologic conditions, which are often related to the repetitive loading tendons undergo during life. In other words, the study of the fatigue resistance of the tendons may provide information about the etiology of these pathologies. The elastic strain limit corresponds to the point after which micro-damage in the tendon starts. Thus, the prediction of this limit and its use in the design of fatigue loading protocols, may benefit the understanding of the onset and evolution of damage which is intimately related to the repair capacity of the cells. The variability of the elastic strain limit between different individuals makes it difficult to choose the applied load in these tests. This thesis shows a possible approach to predict the elastic strain limit based on a point-wise comparison of the sample's stress- strain curve to a set of N number of failure curves from a database that was constructed for this purpose. The accuracy of the method proved to be statistically significantly ($p < 0.05$) higher than other methods that were evaluated. It was also shown that it could be applied to predict the elastic strain limit of other species such as the horse's superficial digital flexor tendon which together to the human Achilles tendon are the most injured between species. The main advantage of this method is that the higher accuracy comes along with a certainty that every prediction will be carried out, in contrast to other methods where some obstacles may render missing predictions. Finally, the smallest strain percentage up to which the sample's stress-strain curve was used for the prediction, proved to be sufficient for obtaining similar accuracy as that with the highest strain percentage tested, with the only requirement of a moderately higher number of failure curves against to which it should be compared.

Achilles tendon injuries are very common among athletes (Schepsis et al. 2002, Matthew B. Werd 2007, Shannon 2011) with an incidence of 11 in 100,000 per year (Clayton 2008) and such injuries most commonly affect middle-aged athletic men (Dudhia et al. 2007, Matthew B. Werd 2007).

One of the main risk factors leading to these injuries is overuse (Flick et al. 2006, Jung et al. 2009, Thornton and Hart 2011). It has been seen that if force is repeatedly applied without giving the tendon time to recover, a degenerative condition will develope and the tendon will become more susceptible to failure even when submaximal loads are being applied (Pekka Kannus PhD, László Józsa, M.D., PhD. 1991, Thornton and Hart 2011). This repetitive loading may include abnormal mechanical loading such as changes in magnitude, frequency, duration or direction (Thornton and Hart 2011). Moreover, other risk factors such as age, vascular supply, training errors, malalignment, flexibility and strength deficits may also contribute to the origin of chronic tendon injuries (Almekinders and Temple 1998). Nonetheless, there is a lack of understanding of the aetiology of overuse injuries, which results in conflicting diagnosis (Almekinders and Temple 1998, Riley 2004).

The degenerative condition preceding the injury is known as tendinosis. It is presented as a group of varied morphological, structural and phenotype changes such as cell rounding (Graham Riley 2008), collagen disorientation and fibre separation(Khan KM 1999), focal variations in cellularity and vascularisation and an increased amount of noncollagenous matrix such as a higher volume density of GAG-rich areas (Movin T Reinholt FP, Rolf C. 1997). Furthermore, mechanical changes such as a decrease in Young's Modulus (Thornton, Shao et al. 2010) are also characteristic of tendinosis.

In the relevant literature there are three main theories to explain the rupture of tendons: a mechanical, a vascular and a neural theory (Riley 2004). The first one is based on the consideration that repetitive microtrauma is the cause of the lesion, analogous to fatigue failure in most materials (Riley 2004, Dudhia et al. 2007). It is assumed that microtrauma, represented by matrix damage, overwhelms the capacity of cells to repair any structural defect (Riley 2004). Furthermore, microdamage such as collagen fiber damage and cross-link rupture can make fibers slide over each other, denature, become enflamed and cause pain (Devkota 2007). This theory is consistent with the increased incidence in relation to age and the presence of degeneration predominantly in the active population but it does not explain by itself the fact that pain is not always present (Rees et al. 2006b).

On the other hand, the vascular theory states that a decrease in circulation as a consequence of ageing, vascular disease, or trauma leads to hypoxia and reduced number of living cells (Riley 2004). Nonetheless, it is often shown that chronic lesions present an increase in vascularity as well as in cellularity (Aström M 1995, Movin T Reinholt FP, Rolf C. 1997). The third theory, the neural

theory, consists of the hypothesis that chronic overuse may lead to excessive neural stimulation and subsequent release of mediators involved in mast cell degranulation which leads to the activation of pain pathways (Rees et al. 2006a). However, the fact that not everyone with tendinosis has pain represents a downside of this theory.

The above leads to tendinosis being considered as having a multifactorial nature (Jung et al. 2009, Andersson and Patrik Danielson 2010). However, the mechanical theory may represent a core link between the other two theories since mechanical loading may affect both nerve endings and blood vessels within the tendon. Furthermore, it is hypothesized that certain loading patterns should be responsible for the morphological, structural and phenotype changes mentioned above. Nonetheless, in order to elucidate the compex relationship that exists between them, the concept of microdamage has to be further studied (Devkota 2007) with a focus on the early stages of the problem (Almekinders and Temple 1998, Fung and Wang 2010).

Some experiments have studied the fatigue behaviour of the tendon with different loading settings and with different specific goals (Ker et al. 2000, Fung and Wang 2010, Zee et al. 2000, Pike et al. 2000, Dudhia et al. 2007). Only few of them have focused their attention on the early stages of the loading (Hui et al. 2010, Fung and Wang 2010, Nakama and King 2005). However, the applied load is always in terms of the ultimate tensile load and applied equally to all the tendons in the experiment. This loading protocol does not take into consideration the variability that may exist between individuals; variability that can also be found even within the same tendon (Sharma and Maffulli 2005, Thorpe et al. 2010) . This means that the applied load may lie at different distances from the elastic limit (inflection point in the stress-strain curve) in each tendon and the biological elements involved in that part of the stress-strain curve are not the same for all samples during the fatigue loading. Then, it is important to be able to predict the elastic limit in order to apply the load at the same distance with respect to this critical point.

For example, all tendon explants may be loaded at the same strain percentage points either below, at or just above their respective elastic limit and the differences in mechanical and biological changes in the short term between these three types of loading could be studied. In addition, the moment at which the accumulated microdamage causes significant changes in each case may help in understanding the difference in the onset of symptoms between individuals or establish a path linking the patient-dependent presence of pain.

The relevance of the study around the elastic limit is related to the physiological loading the tendon undergoes in real life during different activities. The ultimate tensile load of the tendon of about 100 MPa (Ker et al. 2000, Dowling and Dart 2005, Kongsgaard and Aagaard 2005, Rees et al. 2006a) and the load that has been measured during walking (57 MPa) in the human Achilles tendon (Wren 2001)

suggest that even by walking this load may lie just above the elastic limit. However, this might not be the case for every person and may represent one key aspect on why some sedentary persons develop tendinosis (Matthew B. Werd 2007) and others do not or why just one of two persons in the same sports team performing the same exercises and the same warm up, suffers Achilles tendon rupture.

Thus, one of the aims of this thesis was to obtain a method to predict the elastic strain limit which in the stress-strain curve corresponds to the strain when the Young's Modulus starts to decrease from its maximum value (sE_{max}). This method should work independently of the age of the individual which implies that the mechanical properties of the analyzed tendons may vary (Pike et al. 2000, Dudhia et al. 2007). In order to develop this method, *in-vitro* experiments were carried out with porcine superficial and deep digital flexor tendons. These tendons may be considered analogous to the human Achilles tendon due to their position in the pig leg distal to the Calcaneus (J.TM. van Schie 2012). The tarsal joint in the pig approximates 150° while in the human it approximates 90° (J.TM. van Schie 2012). Then, the prediction method was applied to superficial digital flexor tendons (SDFTs) of horses of different ages. The SDFT in the horse is similarly to the human Achilles tendon, the most injured tendon in elite horse athletes (Thorpe et al. 2010). Finally, a series of fatigue tests were carried out with porcine SDFTs and DDFTs where the prediction method was used to decide the load that had to be applied for each tendon. The load was applied below the elastic limit and the strain rate used was that estimated for walking. Both settings were selected as a lower limit case of the physiological loading the human Achilles tendon undergoes and as first approaches to the study of the relevance of the elastic limit in tendinosis due to the underlying micro-structural mechanisms that it represents.

2 MATERIALS

The material used can be divided into experimental samples, handling tools, and the tendon loading device (TLD).

2.1 *Experimental samples*

SUPERFICIAL AND DEEP DIGITAL FLEXOR TENDONS The experimental samples used were the superficial (SDFT) and deep (DDFT) digital flexor tendons of the hindlimbs of Yorkshire pigs. These are fast growing pigs (Ezekwe MO 1975) and according to the weights of the pigs (35 kg to 54.9 kg), their estimated age was between (4 – 6) months (Bell 1964).

A total of 97 explants were obtained from these tendons, of which 40 were isolated from a SDFT and 57 from a DDFT.

SUPERFICIAL DIGITAL FLEXOR TENDON OF THE HORSE One SDFT obtained from the forelimbs of one Frison horse was used to test the interespecies suitability of the two best prediction methods. The age of the Frison was not known but according to the mechanical properties obtained with the failure tests, it could be estimated that the SDFT belonged to an adolescent horse.

2.2 *Tendon loading device*

The Tendon Loading Device (TLD) comprises hardware and software components. The hardware could be further divided in mechanical and electronic components and the software in EPOS and Labview interfaces.

2.2.1 *Hardware : Mechanical*

The TLD works under the principle of an eccentric wheel (Figure 2a) which controls the applied displacement to the explant. The explant is placed inside a chamber (Figure 2b) capable of containing medium during fatigue loading.

2.2.2 *Hardware : Electronics*

The electronic components of the TLD consisted of: amplifier, displacement sensor from ETI, force sensor from Burster, DAQ Labview card, Maxon motor controller and DC motor from Maxon Motor.

The resistance tolerance of the displacement sensor was of 5%, while the linearity tolerance was of 0.5 to 1.5%. The measurement error (combined value for nonlinearity, repeatability and hysteresis) for the force sensor was of ±0.15% of the full scale (the full scale is 10 V for 500 N) for the range above 20 N and of ±0.2% for the range below 10 N. Thus, there was an error of around 0.015 V and 0.02 V, respectively. Further characteristics of the motor and force sensor can be found in Appendix C.1.

2.2.3 *Software*

EPOS INTERFACE The EPOS interface (Figure 4 was used to control the velocity of the motor through the RPM value which had to be introduced in the program. A transmission factor of 51 had to be taken into account when introducing the RPM value. Then, for any desired frequency (Hz), the following calculation had to be done in order to find the RPM value:

$$RPM = f * 51 * 60$$

LABVIEW The custom-made LabView interface consisted of two parts:

1. The front panel which was the user interface (Figure 5). A detailed description of its components can be found in Appendix A.1.3.
2. Block diagram: contained all the programming which included the data acquisition blocks, the conversion from voltages to load and displacement values, the calculation of the stiffness and the display of the graphs (Figure 6).

3 METHODS

The project can be divided into three stages:

1. Prediction of the elastic limit
2. Interespecies application and
3. Fatigue loading

3.1 *Prediction of the elastic limit*

The steps followed in this stage were:

1. Tendon explants isolation

2. Failure tests
3. Comparison of different approaches to predict the elastic limit

3.1.1 *Tendon explants isolation*

The isolation of the explants requires of three steps:

1. Washing and disinfection with 70% EtOH of the pig leg.
2. Deskinning and cutting into explants: first, the leg was deskinned with a scalpel. Then, a piece 7.57 cm length corresponding to the central portion of the complete SDFT and DDFT was cut using a custom-made device. Next, the isolated pieces were further cut into explants of 2 mm width. The depth depended on whether it was a SDFT or a DDFT with mean values of 2.63 mm and 3.61 mm, respectively. In total 40 SDFT and 57 DDFT explants were isolated.
3. Storage of the explants: the explants were stored at $-20\,^{\circ}\mathrm{C}$ until the loading test was performed.

For a detailed description refer to Appendix A.2.1.

3.1.2 *Failure tests*

The aim of the failure tests was to obtain the stress-strain curves of the 97 explants that were previously isolated. Once the information of the complete failure curve had been obtained, further processing could be done with just a fraction of the curve. This fraction would emulate the loading of an experimental sample (explant) just up to this point. The elastic limit of this explant would be known and therefore, the accuracy of any prediction method could be evaluated.

The failure tests consisted of a preconditioning phase and the failure test itself. Each explant was preconditioned with 10 cycles (Aaditya C Devkota 2003) at 3% strain (Gerco Bosch1 2009). The RPM used was 1530 which gave a frequency of 0.5 Hz.

Regarding the failure test, no prestrain was applied and the strain rate used was of $8\%\,s^{-1}$. This is not a loading rate used for quasi-static loading, but it had to be in agreement with the strain rate that would be used for the fatigue tests. For a detailed description refer to Appendix 3.1.2.

3.1.3 *Determining the elastic limit*

The elastic limit, the focus of attention of this thesis, corresponds physically to the stretching point after which microdamage starts (Denoix 2002). This means that the elastic behavior ceases and small microruptures can be seen in the inner structure due to the slippage of interfibrillar cross-links and subsequent dissociation of fibrils (Denoix 2002).

Mathematically, the elastic limit corresponds to the inflection point of the failure curve. This means the moment at which the Young's Modulus stops increasing and starts to decrease which occurs long before reaching the yield point. It is determined by finding the maximum Young's Modulus (E_{max}) of the entire failure curve. Once found, the variable of interest was the strain at this point (sE_{max}) in order to decide which would be the applied strain. A numerical approach was used to find sE_{max} . For a detailed description refer to Appendix A.2.3.

3.1.4 *Comparison of different approaches to predict the elastic limit*

Three different approaches to predict the strain value at the maximum Young's Modulus (sE_{max}) were compared in order to assess which of them provided the more accurate prediction. All methods were implemented in Matlab.

SINGLE STRAIN VALUE USED AS A PREDICTION OF THE ELASTIC LIMIT The first approach consisted of using one single value of strain as the sE_{max} for all explants. This means that no individual prediction would be done, but that just one value would be used to describe the sE_{max} of the 97 explants.

This test was done in order to be used as a reference to evaluate the rest of the prediction methods. In other words, it would be useful to assess if any of the other approaches could improve the prediction based on the mean absolute percentage error (MAPE) (All data refering to the corresponding RMSE from every method herafter can be found in Appendix A).

As explained in the Failure tests section, the actual sE_{max} of each of the explants' stress-strain curves were already known since the complete stress-strain curves were obtained with the failure tests. Different fixed strain values representing the general sE_{max} were tested. These values were contained in a strain vector starting from 1% below the lowest sE_{max} (3.1%) between the set of 97 explants, with an increment of 0.1% up to 1% above the maximum sE_{max} found (11.97%), i.e. from 2.1% to 12.97%. Then, the accuracy of using each of these fixed strain values was assessed by obtaining the mean ± SD of the absolute percentage error for the 97 explants.

EXTRAPOLATION OF THE SAMPLE'S STRESS-STRAIN CURVE The second approach that was tested was the extrapolation method in which just a fraction of each of the 97 explants' stress-strain curve was used as if it were the curve obtained from a single loading up to that strain percentage. Fractions up to 5%, 6% and 7% were analyzed. These strain percentages were selected since they all lay below the mean sE_{max} of the 97 explants which was found to be 7.19%. For those explants for which their sE_{max} lay already above of any of the analyzed strain percentages, the prediction would

consequently not be carried out. The increase in the strain percentage had the purpose of evaluating if the error decreased; however this would not strictly mean that the error converged for the same curves since the number of curves at each strain percentage varied. Thus, the results would indicate up to which percentage it was enough to analyze in order to get an accurate prediction. The lower the better since this way there is a lower probability that the sE_{max} of the sample is exceeded.

Then, after extracting the coefficients of the corresponding fraction of a failure curve, a strain vector up to any strain value greater than the greatest available (5%, 6% or 7%) could be used to extrapolate the missing stress-values. The mean failure strain (11.37%) and the maximum failure strain (16.38%) between all explants were used as the end values of this extrapolation vector and the results with each of them were compared.

The extrapolation was performed with three different types of curves:

1. Polynomial curves of nth degree with n varying from 3 to 8.
2. Gaussian curves of first to third order.
    - An explanation of the consideration of this type of curve is given in Appendix A.2.3
3. Fourier series of nth degree with n varying from 2 to 4.

Once the extrapolation was performed, the sE_{max} of the newly obtained complete stress-strain curve was determined and compared with the actual value of the corresponding explant.

Finally, the mean ± SD absolute percentage error was obtained for each of the strain percentages analyzed (5%, 6% and 7%).

SHAPE-BASED COMPARISON (SBC) OF STRESS-STRAIN CURVES This method performs a point-wise comparison between two stress-strain curves, one corresponding to that of the experimental sample, and another to each of a group of stored failure curves (this group will be referred to as database hereafter). Thus, it takes into account any variation in shape along the trajectory of the two stress-strain curves being compared. The sE_{max} of the stored curves is used for the prediction which was carried out as follows:

1. The 97 failure curves were stored in the form of the coefficients of the fit of two or three Gaussians (Figure 17). The coefficients would later be used to determine the stress values of the failure curves at the same strain points available from the measurement data of the explant for which the sE_{max} needed to be predicted.
2. Then, the sE_{max} of the fit of all curves was determined and stored together with the corresponding failure curve.

3. Next, the comparison between both curves was made by determining the RMSE error between the stress values of both curves. After comparison to all the failure curves in the stored database, the sE_{max} of the failure curve for which the smallest RMSE error was obtained was assigned as the predicted sE_{max} of the sample (Figure 18. The assigned sE_{max} is shown in color blue-green).

The analysis was, similarly to the extrapolation method, implemented with 5%, 6% and 7% of the sample's stress-strain curve.

The difference between the minimum and maximum sE_{max} in the database of 97 explants is of 8.87 percentage points which could allow for a maximum error of 286%. In the context of the shape-based comparison method, it is expected to avoid an error of this magnitude by finding the closest curve. However, the high variability in sE_{max} leaves this method open for any adjustment since finding the closest shape limits the solution to just one option corresponding to the sE_{max} of this match. Thus, a slight variaton of the method where the mean of the sE_{max} of the n closest curves was assigned as the sE_{max} of the sample was also tested and compared to the method using one single curve as previously explained. By considering the n closest curves to the sample's curve, the expected problem of the divergence of the sE_{max} of the matched failure curve from the sample's sE_{max} may be avoided. This is possible since the shape of the fraction analyzed may be similar for multiple curves but the direction followed by each of them may differ. The leave-one-out test principle was used to analyze the accuracy of these predictions methods.

Leave-one-out test with complete set of 97 curves Each of the 97 failure curves was used as an experimental sample. This means that each one of these curves was taken out of the database of 97 curves (Figure 19) and compared with the remaining 96 curves as shown in Figure 20. The comparison was done between the fractions up to 5%, 6% or 7% of the extracted failure curve, in this case called the sample, and the same part of the 96 failures curves i.e. up to 5%, 6% or 7%, respectively. Variations of this test case where different database sizes were used to find out whether there existed an optimum database size that would consistently give accurate results can be found in Appendix A.2.3.

3.2 *Interspecies application*

3.2.1 *Prediction of sEmax of horse tendon explants*

One SDFTs of the Frison horse was isolated and cut into several explants as previously explained for the pig tendons. The SDFT was cut into 15 explants and it was stored in a freezer at −20 °C until loading took place. The loading conditions were the same used for the failure tests of the pig explants (Section 3.1.2).

Then, the corresponding stress-strain curves were obtained with the previously measured CSA and length between clamps at the beginning of the loading.

Next, the prediction method that gave the smallest MAPE would be tested with the horse tendons. Furthermore, it would be implemented with and without normalization of the pig and horse stress-strain curves in order to assess if this was a necessary step. The normalization would be done in two different ways. The stress-strain curves would be normalized either with respect to the UTS and the failure strain or with respect to the UTS and the sE_{max}.

3.3 *Statistical Analysis*

In order to assess for statistical significance between the different methods a significance level of 0.05 was used. Paired samples t-tests and one-way repeated measures ANOVA were performed when normality was complied. Otherwise, related samples Wilcoxon signed rank tests and Skillings-Mack test were performed. Greenhouse-Geisser correction was applied whenever sphericity was not fulfilled and Bonferroni correction was used for Post-hoc pairwise comparisons.

4.1 *Prediction of the elastic limit*

4.1.1 *Failure tests*

PIG SUPERFICIAL AND DEEP DIGITAL FLEXOR TENDONS Table 4 shows the mean values for the failure load, ultimate tensile stress (UTS) and cross-sectional area of the SDFT and the DDFT; Table 5 shows the mean values for the strain at the end of the toe region, strain at the maximum Young's Modulus, yield strain and failure strain; and Table 6 shows the the mean values for maximum Young's Modulus, the Young's Modulus of the elastic region and the Young's Modulus of the entire quasi-linear region which goes from the end of the toe region up to the yield strain.

The mean UTS, failure strain and sE_{max} of the 97 explants altogether were 17.49 MPa, 14.4% and 7.4%, respectively. The UTS of four explants out of the 97 explants lay above two standard deviations from the mean, while no outlier was found for the failure strain. The UTS outliers belonged to SDFT explants except for one DDFT explant. There was only one outlier for the sE_{max}, which corresponded to the same DDFT explant from the UTS outliers.

Even though the loading conditions used (strain rate: $8\% s^{-1}$) did not correspond to quasi-static conditions with a characteristic low strain rate, they were in the lower range of what can be considered as a moderate strain-rate (Ming Cheng and Weerasooriya 2009). Thus, no significant variations from the reported data in the relevant literature were expected for Young's Modulus and UTS. As explained in Appendix A.1.1, the Young's Modulus for newborn mammals may lie around 0.16 GPa, for infants around 0.33 GPa and for adults around 1.5 GPa. Thus, the measured Young's Modulus of 0.294 ± 0.149 GPa for the SDFT and of 0.251 ± 0.084 GPa for the DDFT agree with the fact that the pigs that were used in the experiment were $4-6$ months old.

It can be observed that the mechanical properties of both groups agree with the fact that they are elastic energy-storing tendons. However, the SDFT explants are more elastic than the DDFT explants since they show higher strain at the end of the toe region, higher strain at E_{max}, higher yield strain and higher failure strain. The higher end of the toe region can be explained by the differences in the crimp patterns of the tensile regions of both tendons. The SDFT shows a well-defined wave-like pattern, while the DDFT shows a more uniform pattern along its longitudinal axis (Figure 22) (V.L.C. Feitosa 2006).

HORSE SUPERFICIAL DIGITAL FLEXOR TENDONS Table 7-9, show the mean values for the same mechanical properties as for the pig tendon explants.

The outliers of these meaurements were one explant whose sE_{max} and failure strain were above two SD from the mean and one explant whose UTS was below two SD from the mean.

4.1.2 *Single strain value used as a prediction of the elastic limit*

A minimum mean absolute percentage error (MAPE) of 27.57% was obtained when using a single strain value of 6.2%. The standard deviation of the MAPE at this point was 18.60%. Furthermore, it can also be observed that the interval [MAPE - SD, MAPE + SD] showed a minimum at a strain value of 5.7% which is slightly to the left of the minimum MAPE. The MAPE and SD at this point were 28.19% and 16.43%, respectively (Figure 23).

4.1.3 *Extrapolation of the sample's stress-strain curve*

The total number of attempted predictions which exclude those curves for which their sE_{max} was already passed at each of the percentages analyzed (5%, 6% or 7%) were 79, 65 and 53, respectively. Table 10 shows the results for the accuracy of the prediction when the mean failure strain was used as the end value of the extrapolation vector. These results were in all cases smaller than those for the maximum failure strain (not shown) for all the types of curves (polynomial, Gaussian and Fourier series). The results for any of the extrapolation curves used showed a decreasing MAPE from the 5% strain to the 7% strain used.

Table 11 shows the following statistics: 1) percentage of predictions that could be carried out, 2) percentage of overpredictions out of those in 1 and 3) percentage of extrapolation curves out of those in 1 that became negative before the end of the extrapolation vector.

The predictions that could not be carried were due to lack of an inflection point. The smallest order reported for the polynomial extrapolation is 4 since no more than 3 predictions could be performed for any of the strain percentages for a third order polynomial. In addition, some extrapolated curves reached negative values changing direction and thus shape, from the expected one sometimes at a very early stage of the extrapolation.

On the other hand, by looking at the MAPE ± SD alone (Table 10), it may seem that the best options for the extrapolation were the gaussian curves order 2 (Gauss 2), polynomials order 4 and 5 (Poly 4 and 5) and fourier series order 2 (Fourier 2) and in particular the last two which showed the lowest MAPE ± SD. The MAPE results were analyzed with a Skillings-Mack test and indicated that using gaussian curves and fourier series, both of second order as the extrapolation curves renders statistically significantly different ($p < 0.001$) prediction erros for 5%, 6% and 7% in any of the possible

pairwise combinations. Furthermore, for extrapolation curves using polynomials of fourth and fifth order the results were also statistically significantly different ($p < 0.001$) except for a non-significant difference between 5% and 6% strain.

It was also assessed which extrapolation method yielded better results for each of the strain percentages. The Skillings-Mack method revealed that the difference between any of two methods was significant ($p < 0.001$) when up to 5% and 7% strain of the stress-strain curve were used but not with 6% strain, where the difference between Fourier 2 and Poly 5 was not significant ($p = 0.254$). Thus, according to this analysis, the best extrapolation method for each of the three strain percentages considering Table 10 was Poly 5 for 5%, Fourier 2 for 7% and either Fourier 2 or Poly 5 for 6%.

However, if the complete performance of the extrapolation is considered (Table 11), it can be seen that a trade between accuracy and predictions possible may have to be done. The sum of two gaussians had the highest percentage of predictions that were possible to carry out as well as the lowest percentage of overpredictions and except for 6% strain, the lowest magnitude of the MAPE of these overpredictions between all the types of curves previously mentioned (Gauss 2, Poly 4 and 5 and Fourier 2). In addition, it also had the lowest percentage of curves that became negative before the end of the extrapolation.

4.1.4 *Shape-based comparison (SBC) of stress-strain curves*

LEAVE-ONE-OUT TEST WITH COMPLETE SET OF 97 FAILURE CURVES

Closest curve Table 12 shows how with this method both the MAPE and its standard deviation decreased as the strain percentage analyzed increased.

The percentage of predictions that lay above the real sE_{max} of the sample (Table 12) represent for the three strain percentages near half of the predictions out of 79, 65 and 53 predictions, respectively. Thus, these high percentages represent the ratio of predictions where microdamage may not be avoided if the load is applied certain percentage below the predicted sE_{max}which may still lie above their actual sE_{max}.

N- closest curves Figure 29 shows the linear correlation between the MAPE obtained with the N-closest curves method and the number of curves. The higher the number of curves the lower the MAPE. Both the MAPE and the SD showed a decreasing trend with increasing strain percentage used as shown in Table 12.

Comparison between Closest and N-Closest for the same strain percentage A related samples Wilcoxon signed rank test indicated that the MAPE obtained with the N closest curves method was

significantly smaller for each of the three strain percentages (Z = -3.064, p = 0.002; Z = -2.545, p = 0.011 and Z = -2.527, p = 0.011, respectively). On the other hand, a slight modification of the N-closest curves method into a mechanical representation of probability was done in order to consider prevision, i.e. predict the sample's sE_{max} without the information of the distance of the sE_{max} of the N-closest curves to the sE_{max} of the sample: a weighted average of the N-closest sE_{max} where the weights corresponded to: 1) their probability out of the discrete probability distribution of the sE_{max} of the 97 samples in the database, 2) the inverse of the normalized RMSEs corresponding to those RMSEs with which the N-closest curves were determined, 3) the combination of 1 and 2 by considering them as both dependent and independent events. All of these approaches yielded similar but not better results than the one considering just the average value of the sE_{max} of the N-closest curves.

Comparison between strain percentages for Closest and N-Closest approaches A Skillings-Mack test determined that the mean absolute percentage error (MAPE) differed statistically significantly between the three strain percentages (5%, 6% and 7%) for the prediction method using only one curve for the estimation of sE_{max}. Post hoc tests using the Bonferroni correction revealed that using information of the stress-strain curve up to 6% allows for obtaining a smaller MAPE than up to 5% (13.45±10.6 % v.s. 14.39±11.26 % , respectively) which was statistically significant ($p < 0.001$). The same situation ocurred with 7% when compared to 6% (12.32±9.6 % v.s. 13.45±10.6%, respectively). On the other hand, the method using more than one curve for the estimation of sE_{max} had minimum values of the MAPE at N = 32, N = 17 and N = 11 for 5%, 6% and 7%, respectively. These values corresponded to 9.96%, 10.21% and 8.14% respectively. Post hoc tests showed that at N = 11, the MAPE using 7% strain was statistically significantly lower than that with 6% and 5% but as the N increased the MAPE obtained with 6% strain became consistently smaller and the difference with that error was not significantly different anymore. After this point, the error with 5% decreased notoriously such that at N = 32, the was no significant difference between any of the strain percentages used ($p = 0.89$).

4.1.5 *Comparison between prediction methods*

The Skillings-Mack test was used for the comparison between prediction approaches. Only Gauss 2 from the extrapolation method was used for the comparison due to the lowest number of missing values in the total number of predictions w.r.t. to the other extrapolation curves. The two approaches of the shape-based comparison method were compared to the reference analysis for the case when a single strain value of 6.2% was used to estimate the sE_{max} of all the curves giving a MAPE ± SD of 27.57 ± 18.60%. All methods had a significantly ($p < 0.001$) lower MAPE ± SD w.r.t. the reference

analysis at the three strain percentages except for the extrapolation method Gauss 2 at 5% strain percentage with a MAPE±SD of 27.48 ± 13.22%.

4.2 *Interspecies application*

As shown in the results for the comparison between the prediction methods, the most accurate prediction method was the shape-based comparison between stress-strain curves. Thus, this was implemented for the prediction of the sE_{max} of the horse tendon explants in all its variants, i.e. using the best match between all curves and using the n closest curves. The latter approach used a complete database of 97 curves and the former used both:

1. A complete database of 97 pig failure curves and
2. Databases of different sizes (5 to 95) constructed with randomly selected curves .

Then, the normalized pig stress-strain curves were fitted with a sum of two or three Gaussians in order to proceed with the prediction.

Comparison between Closest and N-Closest for the same strain percentage When the two alternatives of the shape-based comparison method were compared, no statistically significant difference was found between the two of them for either without normalization of the stress-strain curves or normalization w.r.t. the mean UTS and mean failure strain of each species. However, a repeated measures t-test showed that the MAPE of the N-closest curves approach (11.21±7.27%) was significantly (t = 2.285, p = 0.041) lower than the one of the closest curve approach (19.15±14.31%) in the case in which normalization w.r.t. the mean UTS and mean sE_{max} of each species was used together with up to 3% of the horse's stress-strain curve.

Comparison between strain percentages for Closest and N-Closest approaches Using up to 3% percent strain of the horse failure curve yielded better results than using 2% percent for all cases except for the case of normalization w.r.t. the mean UTS and mean sE_{max} of each species. An analysis of the mean ± SD of the pig and horse normalized failure curves w.r.t. sE_{max} was performed. Despite the overlap in the horse and pig curves (Figure 30), there still exists the possibility that outliers appear, which was the case, due to the high variability in sE_{max}.

The statistical analysis was performed for the following cases: 1) the MAPE for the closest curve approach of the shape-based comparison method, 2) with the MAPE at the N (number of closest curves) corresponding to the smallest MAPE between 2% and 3% and 3) between the minimum MAPE of 2% and that of 3% independently of the N value.

The Skillings-Mack test showed that when no normalization was applied the difference between the results for 2% and 3% were non-significant for cases 1-3 as well as those for normalization w.r.t. UTS and sE_{max}. for case 1. Furthermore, normalization w.r.t. UTS and failure strain yielded MAPEs satistically significant ($p < 0.05$) lower for 3% than for 2% for cases 1-3. Finally, normalization w.r.t. UTS and sEmax yielded significant ($p < 0.05$) lower MAPEs for 3% for cases 2-3.

Comparison between normalization and without normalization Finally, a repeated measures ANOVA test with a Greenhouse-Geisser correction determined that the MAPE differed statistically significantly between the normalization approaches in each of the prediction approaches of the shape-based comparison method. Two different N values for the number of closest curves were analysed such that the minimum errors for both 2% and 3% were considered. Post hoc tests using the Bonferroni correction showed that for 2% there was a significant difference (for mean values refer to Table 13) between normalization w.r.t. UTS and failure strain and without normalization for both N = 25 ($p = 0.019$) and N = 28 ($p = 0.006$) and between normalization w.r.t. UTS and sEmax and without normalization for N = 28 (0.039). In general, no significant difference was found between normalization approach in any case, i.e. for both closest curve and N-closest curves prediction approaches.

Two methods with their variations were tested in their capability to predict the sE_{max} of any tendon without regarding the species from which they come from. They were compared to a reference test case in which a predefined sE_{max} was considered as the sE_{max} of the sample in order to asess the need for prediction.

First, the extrapolation method was analyzed and several pitfalls in the performance were encountered such as lack of inflection point to calculate the sE_{max}, high percentages of overpredictions and negative values in the extrapolation curves. It was seen that in terms of accuracy Fourier 2 and Poly 5 gave the most accurate predictions but that if performance, such as number of predictions that were carried out, was also considered, Gauss 2 would be the option to use with a trade off in accuracy. However, none of the extrapolation curves used was exempted from undesirable missing predictions besides those included by design (those cases at which the prediction was not performed since the sE_{max} had already been exceeded). In addition, the shape of the sample's curve or some non-smooth features might have caused the coefficients to cause some instabilities in the extrapolation curves. These sometimes changed direction even before arriving to the end of the sample's stress-strain curve from which the information was known through the coefficients.

This method also showed cases in which the standard deviation of the prediction obtained with the sample's stress-strain curve up to a certain strain percentage (e.g. 5%) was sometimes lower than for a higher strain percentage (e.g. 6%). The reason for this might be that despite the decrease in the MAPE with increasing strain percentage (5%, 6% and 7%) observed in all cases, outliers may have a greater effect in the variability than in the mean and there were many sources of outliers that may have dominated in certain cases.

If the extrapolation method had proven to be the most accurate, the advantage would have had been that in future research, only the stress-strain information of the sample would have had to be processed to be able to obtain a prediction of sE_{max} and no set of extra curves would be needed to be used for the prediction as was the case for the shape-based comparison method.

On the other hand, the closest and N-closest curve approaches, variants of the shape-based comparison method do not present the problem of missing predictions. Furthermore, the N-closest curve method shows an improvement in the accuracy as the number of closest curves increase. Despite the fact that the percentage of overpredictions for the closest curve approach is higher (around 45% of overpredictions) than for the extrapolation method (around 10-20% of overpredictions) , the magnitude of these were close to the MAPE±SD of the total number of predictions, which might be due to the fact that they did not constitute outliers but formed part of most of the distribution. In contrast,

for the N-closest curve method, the MAPE±SD of the overpredictions were around 3-4 percentage points higher than for the total predictions for 5% and 6% strain. Nonetheless, from the overall results, the N-closest curves approach proved to be the most accurate and reliable method. A fraction of the sample's stress- strain curve up to 5% may be the best option to carry out the predictions since the only requirement to attain an accuracy that does not statistically significantly differ from the one attained with 7% strain is to work with a higher, plausible number of N-closest curves equal to 32. Furthermore, the reason for the variations of this method not to yield improved results even though they approached the problem considering probabilities might have been that the principle of considering the N-closest curves already circumscribed the solution to a very small area.

When the shape-based comparison method was applied to another species, there was no significant difference of using the closest or the N-closest approach either without normalization or with normalization w.r.t. the mean UTS and mean failure strain of each species. However, normalizing w.r.t. the mean UTS and the mean sE_{max} did provide an advantage to using the N-closest method w.r.t. the closest curve approach.

As expected, for every method used, the smallest mean absolute percentage error corresponded to when up to 7% strain of the sample's stress-strain was used, followed by that obtained with 6%. As previously mentioned, this decrease in the magnitude of the error cannot be strictly considered as a convergence trend since the number of sample's for which the sE_{max} is predicted at each of the strain percentages (5%, 6% or 7%) varies from one to the other. However, in the case of the N-Closest curves approach of the shape-based comparison method, the fact that with 5% strain, the MAPE was not statistically significantly higher than the one obtained with 6% and 7% strain, comes close to the aim of obtaining a reliable percentage error with the lowest percentage strain used. The reason is that the lower the fraction of the stress-strain curve used, the higher the number of samples of which the sE_{max} need to be predicted. For both, experimental research and possible future applications in diagnostics and therapy, failed predictions are not acceptable since for the former the number of samples are not always easily accesible and for the latter the quality of the health assistance would be diminished.

A.1 *Materials*

A.1.1 *Experimental samples*

YORKSHIRE PIG*s:* According to an anatomist in the University of Utrecht in The Netherlands, skeletal maturity in pigs is reached at 18 months (Wolschrijn 2011). Furthermore, according to Reiland S. (1978), there is a high increase in weight until around 5 months of age, after which there is an inflection point; thus calling adolescence the period between 5 and 18 months. After 18 months, the weight curve is flattened (Reiland 1978). The pigs used in this experiment are around 4-6 months old. Thus, they are in the transition phase between infant and adolescent pigs. Based on the similarity in mechanical properties between tendons (R. F. Ker 1988; Robert F. Ker 2000; Dowling and Dart 2005; M. Kongsgaard 2005; Rees, Wilson et al. 2006), the study of the tendon of an early adolescent pig represents an opportunity to understand more about the first degenerative changes that may evolve into what in humans is clinically detected in adulthood in the clinics. The symptoms in the human patellar tendon may become overt at young ages of 31 years (K M Khan 1996) and early signs of degeneration have been detected even at an age of 14 years old (Cook JL 2000).

PORCINE SDFT AND DDFT The superficial and deep digital flexor tendons sprout from the distal part of the superficial and deep flexor muscles, respectively. Their function is to extend the hock or knee and flex the digits (Rowen D. Frandson 2009).

Mechanical properties Adult mammalian tendons show Young´s Modulus of around 1.5 GPa above stresses of 30 MPa (Shadwick 1990; M. De Zee 2000). A reported range for this mechanical property lies between 1.2 and 1.8 GPa (Shadwick 1990; Shadwick 1994; M. De Zee 2000; Robert F. Ker 2000). Some studies argue that at least three orders of magnitude higher strain rate may be needed in order to see a difference in Young's Modulus (Ming Cheng 2009). However, other studies show a variation already with an increase in the strain-rate of one order of magnitude if the tissue is well-hydrated (Tammy L. Haut 1997). On the other hand, the generally accepted UTS value describing all types of tendons is 100 MPa (R. F. Ker 1988; Robert F. Ker 2000; Dowling and Dart 2005; M. Kongsgaard 2005; Rees, Wilson et al. 2006), while the reported range lies between 70 and 120 MPa (Shadwick 1990). The failure strain values which have been measured for adult tendons range from 12% to 21% (E. L. Batson 2003; Dowling and Dart 2005). Furthermore, these values are age dependent. A Young's Modulus of 0.16 GPa and 0.33 GPa were measured for pig newborn flexor tendons and 1

month old rat tail tendon, respectively (Shadwick 1990). In terms of UTS, values around 30 MPa were found for 1 month old rat tail tendon as well as for human infant tendons (Shadwick 1990). The elastic limit, the focus of attention of this thesis, corresponds physically to the stretching point after which microdamage starts (Denoix 2002). This means that the elastic behavior ceases and small microruptures can be seen in the inner structure due to the slippage of interfibrillar cross-links and subsequent dissociation of fibrils (Denoix 2002).

Characterization of the Mullin's effect The loading and unloading paths followed by the porcine flexor tendons follow the same trajectory described by Ming Cheng (2009) for bovine flexor tendons: the first unloading curve is well below the first loading path, which means that hysteresis is high; the next loading and unloading paths are slightly above and below the first unloading path, respectively and the same pattern is followed by the subsequent cycles (Figure 1). Ming Cheng (2009) also showed that this behavior can be observed at strain rates three orders of magnitude higher than the one used in this experiment.

A.1.2 *Handling tools / material*

The tools used for the isolation of the explants consist of the following: scalpel, press, surgical pincers and forceps, cotton tablecloths, spaghetti cutter, cut board, test tubes, phosphate buffered saline (PBS) and Dulbecco's Modified Eagle Media (DMEM) enriched with Gentamicin (antibiotic) and Fungizone (antimycotic). The tools used during the loading of the explants were: surgical pincers, sandpaper, PBS and DMEM medium.

A.1.3 *Tendon loading device*

HARDWARE

Hardware : Mechanical The vertical displacement the upper clamp undergoes is determined by the position of the axis of the eccentric wheel (Figure 2a). The maximum vertical displacement obtained when the axis is at one of the extremes is 9.93 cm while the minimum vertical displacement is zero and corresponds to the opposite extreme of the wheel. The tendon explant was placed in the device by means of two removable clamps. The lower clamp was held by a chamber (Figure 2b) which was designed to contain any fluid in fatigue tests.

The greater the desired applied strain, the greater the vertical displacement the upper clamp undergoes. Thus, it was possible that the lower part of the displacement sensor could get detached from

the white chamber, which could interrupt the ongoing measurement. Therefore, the plate atop the displacement's sensor had to be placed accordingly.

Hardware : Electronics The amplifier (Figure 3a) received the signals of the displacement and the force sensor (precision load cell) which were processed in the DAQ Labview card in order to obtain a discrete signal that was sent to the computer for further processing.

The motor used was a DC motor from Maxon Motor. The displacement sensor consisted of a precision linear motion potentiometer from ETI (Figure 3d).

The Maxon motor controller was the connection between the power supply and the work settings for the motor introduced in the computer. Table 1 shows the aim of the three connections of the motor controller shown in Figure 3c.

SOFTWARE The front panel consisted of:

1. The graph of real-time load v.s. displacement
2. The graph of stiffness v.s. number of cycles: in a fatigue test where the applied strain was below the elastic strain limit, the stiffness was calculated with the last 5 (x, y) points, in this case (displacement, load) points, before the peak of each cycle and determined as the slope of the linear fit of these points.
3. Path browser to select the excel file where the measurements had to be written.
4. Save button and alarm button: they allowed the recording of the current stiffness and also signaled the moment in which the stiffness went beyond a critical value, respectively. These buttons were used for the fatigue tests. The critical value was determined after a series of fatigue tests from which the percentage of decrease in stiffness of the first degradation step was determined. The first degradation step was considered as that which occurred after stabilization of the stiffness had been reached following the stress-softening of the first loading cycles.

A.2 *Methods*

A.2.1 *Tendon explants isolation*

The isolation of the porcine and equine explants is described in the following paragraphs:

As a preparation step, the work environment (Figure 9) with all the tools that would be used to deskin the leg (scalpel, press for the leg, surgical pincers, surgical forceps and cotton tablecloths), cut

the tendon into the explants ('spaghetti cutter' and cut board) and organize the already cut explants (test tubes) would be placed on the working table.

WASHING AND DISINFECTION The leg was washed with soap after which it was placed in 1 – 2 L of 70% EtOH for 10 minutes for disinfection purposes (Figure 10).

DESKINNING AND CUTTING Next, the deskinning of the leg was performed with a scalpel in the open air and not under a hood, since sterile conditions during isolation were not required. This was because the focus of study were the mechanical properties of the tissue and the explants were going to be frozen. Then, it was enough to work under clean conditions. The leg was fixed in a prone position with aid of a press that was clamped onto the working table.

After removing the skin together with the superficial fascia, the first tendon exposed (Figure 11), the SDFT of around 13 cm length, had to be cleaned from the paratendon (connective tissue surrounding the tendon). The region of interest of both tendons was the central part of the tendon in the longitudinal direction since it is the one subject to pure tension. The extremes are subjected to both tension and compression or compression only since they wrap around the joint, thus subjected to perpendicular compression forces (V.L.C. Feitosa 2006). The length of the isolated piece of tendon (7.57 cm) corresponded to the length of the custom-made device (*spaghetti* cutter) used for cutting it later into smaller pieces known as explants. The same steps of cleaning and cutting were followed for the DDFT of around 10 cm length (visible part before tarsal joint).

The next step consisted of further cutting the tendons into thin explants so that they would fit in the chamber of the loading device (Figure 12). Depending on the thickness of the tendon was the number of explants that was obtained. When the DDFT was cut, an average of 4 well-conserved explants was obtained, whilst with the SDFT the average was 3 per tendon. The explants may be further cut along their length in order to obtain a higher number of samples. However, the lower the handling, the lower the non-desired effects on the structural integrity.

The distance between the blades was fixed and was 2 mm. However, the depth varied depending on whether the SDFT or the DDFT was cut. The explants that corresponded to the SDFT had an average depth of 2.63 mm, while the explants that belonged to the DDFT group had an average depth of 3.61 mm.

STORAGE OF THE EXPLANTS After isolation the explants were stored at −20 ºC until the failure test was performed. Any cellular activity would be stopped after freezing the tissue avoiding any secretion of degrading enzymes. Furthermore, it has been shown that the duration tendons are

frozen before a failure test does not significantly change the mechanical properties in a failure test (Hirpara, Sullivan et al. 2008).

Each explant was stored in a different test tube with the proper label to be able to distinguish between types of tendon, the leg to which it belonged and other explants of the same tendon (Figure 13).

A.2.2 *Failure tests*

PRECONDITIONING Preconditioning before a failure test is a necessary step such that the fibers untangle and the true mechanical properties can be observed during the test. The values of the loading settings vary through literature but in general the applied strain lies around 3% and the number of cycles lies above 5. The reason of using more than 5 cycles is because during the first loading cycles of a displacement-controlled experiment the tendon will show a pronounced stress-relaxation known as Mullin's effect (Ming Cheng 2009). However, after 5-10 cycles a certain degree of stabilization is already observed (Shadwick 1994; Aaditya C Devkota 2003).

FAILURE TEST A value of $10\% s^{-1}$as reported by (Tishya A.L. Wren 2001) was not selected since it caused instabilities in the measurement values provided by the force and displacement sensors. The strain rate used in this test had to be in agreement with the strain rate that would be used for the fatigue tests. It had to at least lie within the same order of magnitude to avoid significant differences in the stress-strain curve of the single loading up to either 5%, 6% or 7% needed for the prediction of the elastic limit. The strain rate during walking is the lowest physiologically relevant strain rate that could be analyzed. According to the stress level of 57 MPa measured during walking, this activity could already be involved in the initiation of the degeneration of the tendon.

The following steps had to be followed as a preparation for any type of loading, whether it was cyclic (preconditioning or fatigue tests) or just a single loading episode (failure test):

1. Place the axis of the eccentric wheel at the desired position along its diameter. This would allow the desired strain to be obtained by displacing the upper clamp the corresponding vertical distance.
2. Measure the distance between clamps to determine the initial length value necessary for the calculation of the strain. This value changes each time the position of the axis of the eccentric wheel changes. Thus, these two measurements had to be iteratively adjusted to obtain the desired settings that would result in the expected applied strain.
3. Turn the eccentric wheel up to where the upper clamp was at its lowest position in order to start the loading from that point.

4. Clamp the tendon explant using sand paper as an interface. In order to avoid undesired bending of the explant, the upper extreme of the explant was clamped first.
5. Once clamped, the cross-sectional area (CSA) was measured with a digital caliper at the explant's thinnest region with a 0.01 mm accuracy. The shape of the explant's CSA is close to elliptical; thus, the formula used for the calculation was: $A = \pi * a * b$, where a and b are the major and minor radius.
6. Draw a line of indian blue ink on the explant along the edges of the clamps such that any sign of slippage could be detected (Figure 15).
7. Introduce the values of the corresponding RPM in the EPOS interface. The RPM would depend on the frequency of the loading as explained in the Software subsection of the tendon loading device. The frequency would in turn depend on the desired strain rate and the displacement of half-cycle of the upper clamp during loading:

$$displacement = \sin(2\pi f t)$$

$$velocity = displacement * 2\pi f * \cos(2\pi f t)$$

$$strain\ rate = \frac{velocity}{initial\ length}$$

8. Start the measurement in Labview followed by the start up of the motor at the EPOS interface. The load-displacement output was written in an Excel file.

A.2.3 *Comparison of different approaches to predict the elastic limit*

DETERMINING THE ELASTIC STRAIN LIMIT The calculation of the sE_{max}can be summarized as follows:

1. The stress values were obtained by dividing the load vector by the area of the clamped explant at the beginning of the loading. The strain values were determined by dividing the displacement vector by the length between clamps in the initial position.
2. The 97 failure curves of the pig tendons were fitted with a sum of two or three Gaussian curves (See Appendix A.2.3), depending on which gave a better goodness of fit based on the R^2 of the fit. Most of the 97 failure curves were fitted with a sum of three Gaussians (68 curves).
3. The Young's Modulus of the fit was determined by differentiating the function of the fit at the strain corresponding to the middle points between two strain points. The middle points were selected due to the fact that the error converges faster (midpoint approximation; O (h^2)) at this

point, in contrast to if it were assigned to one of the strain points from which it was obtained (backward/forward difference; O(h)).

4. The maximum Young's Modulus was found and the corresponding strain was established as the strain delimiting the elastic region.

FITTING WITH A SUM OF GAUSSIANS The sum of Gaussian curves was considered since the shape of the first half of the resulting curve is very similar to the complete characteristic failure curve of the tendon. In order to decide whether the goodness of fit was appropiate, a comparison to the goodness of fit (based on the coefficient of determination R^2) of other types of curves was performed. The results are shown in Table 3. It can be seen that all the results are very similar with a R^2 close to 1. Since the curve that is being fitted is not periodic, the combination of two and three Gaussians was considered more appropiate than the Fourier series for this purpose. On the other hand, the R^2 of the former is marginally different than that for Poly 6-8 and Fourier 4 orders used (lower by 0.02%). If we consider the fact that the coefficients of the fit are obtained with their respective confidence intervals, that further undermines the slight advantage of the polynomials may seem to have based on the R^2 statistic. Thus, in order to be consistent with the results of the extrapolation method for the prediction of sE_{max}, the combination of two and three Gaussians was selected as to assess the suitability of working with these type of curves.

Extrapolation with a sum of Gaussians A first order gaussian curve is a type of exponential curve but in contrast to a non-gaussian exponential, the curve possesses an inflection point which resembles the behaviour of the stress-strain curve in a tendon's failure test. Thus, different orders of this type of curve were considered as test cases in this method.

A.2.4 *Interespecies application*

The fundament upon which different database sizes (Figure 31) were used for the prediction of the sE_{max} of the porcine stress-strain curves was also followed here. There may exist a database size smaller than 97 that proves optimum in terms of both mean absolute percentage error and standard deviation. This means that it would not be necessary to construct a big database but a smaller size would render statistically similar results.

A.3 *Complementary Analyses*

A.3.1 *Single strain value used as a prediction of the elastic limit*

In contrast to the MAPE, which gives a relative measure according to the point in the x-scale in which the real sE_{max} lies, the RMSE gives an absolute measure of the magnitude of the error. This means how many percentage points away the predictions lies from the real sE_{max}. While it does not reflect the relative importance of the error, it does give a quick idea of the magnitude of the error in question. Figure 24 shows a minimum RMSE of 2.09% which was obtained for a fixed strain value of 7.2% which corresponds to the mean sE_{max} of the 97 explants.

A.3.2 *Extrapolation of the sample's stress-strain curve*

The isolated fraction of a failure curve was smoothed with spans (percentage of data points from the extracted fraction) from 10% to 60% to test if there was an improvement in the extrapolated curve with respect to not using a smoothing step. In other words, the reason was to identify if any of them caused fewer deviations from the expected extrapolation curve and thus render better predictions than they case where they are not used. The span of 0.2 used was the one with which the lowest MAPE and RMSE were obtained over the rest of the spans and with respect to when no smoothing step was used. The small percentage allows for the conservation of the shape of the curve close to the original. However, at the end of the analysis it was concluded that the smoothing span did not have a noticeable influence in the results since the improved results for some curves by using a specific span with respect to other span were counterbalanced with a deteriorated result for other curves when using the same spans (Figure 25).

A sensitivity analysis for the comparison between Gauss 2 and Fourier 2 was carried out for each of the three strain percentages. The reason of just using these two types of curves was that they were the ones that gave the fewest missing values and complied with missing values MCAR and an assumed criteria of less than 40% missing data in order to proceed with the multiple imputation of values. Similar results to those of the Skillings-Mack test were obtained confirming that using Fourier 2 was better than Gauss 2 for the three strain percentages, 5%, 6% and 7%.

A.3.3 *Shape-based comparison (SBC) of stress-strain curves*

LEAVE-ONE-OUT TEST WITH COMPLETE SET OF 97 FAILURE CURVES The RMSE did not show a convergence trend but possessed a minimum when a "loading strain" of 6% was analyzed. If the non-normal distributions of the error for 6% and 7% strain are analyzed (Figure 26), it is observed

that both of them were very similar but the number of predictions that were carried out for 7% strain were fewer than for 6%, which together with the fact that in 23% of the predictions that were carried out for 7%, the absolute percentage error was higher than that obtained for 6%, it can be understood that there RMSE was slightly higher than for 6%.

A.3.4 *Databases of different sizes using randomly chosen curves*

In this test case, different databases of different sizes were generated from curves randomly chosen from the 97 failure curves. The sizes ranged from 2 to 96 curves. The reason to test different database sizes was to find out if there was an optimum size which would consistently give accurate results. Two different approaches were taken with each of the database sizes:

1. Leave-one-out test performed for the chosen curve-set.
2. Complementary curve-set to the chosen one used as experimental samples with the chosen curve-set acting as the database; for example, if the database size was of 10 curves, 87 curves were used as samples.

For both approaches, databases of each size were generated 10 times and the corresponding predictions were performed. This was done to ensure sufficient variability in the curves chosen for a particular size. Each of the 10 times, the mean ± SD of the absolute percentage error and the RMSE were determined. Afterwards, the mean ± SD of the MAPE and RMSE were obtained for each of the database sizes. This last accuracy assessment would indicate which database size provided a more accurate prediction considering the fact that the method was implemented 10 times.

Results

Leave-one-out test (L1OT) The database for which the smallest average MAPE was obtained for the three percentages analyzed (5%, 6% and 7%) corresponded to 20 curves. However, it cannot be said that this was the optimum database size since as can be seen from the graph, the results show an oscillatory outline throughout the database sizes.

In the three cases (5%, 6% and 7%), it can be said that there was no linear dependence between the accuracy of the results and the database size (Figure 27). Thus, no optimum database size was found. However, the minimum average MAPE + SD was found for the last database sizes (95 and 96 curves) due to the more or less constant mean MAPE throught all database sizes and that the SD at these points were the smallest found.

In contrast, when the database size was too small, e.g. 2, the SD was very large as a result of the difference in sE_{max} between the two randomly selected curves. In this case, the shape did not have an influence since there was only one option to perform the match.

Complementary curves to the databases used as experimental samples Figure 28 shows how for small database sizes the standard deviation was higher than for database sizes in the middle of the range. This occurred since a very small number of curves were used to predict the sE_{max} of the rest of the curves. On the other hand, the reason for the standard deviation to increase from half of the graph towards the end is that the lower the number of curves for which the prediction had to be performed, the lower the number of curves that would be considered in the average of the MAPE in each of the 10 iterations. In case the results of some iterations showed a high MAPE because of the previously explained reason, this would be reflected in the standard deviation of the database size. In other words, the right side of the graph shows how the error may behave in an isolated case of a real experiment when one sample is being tested. Furthermore, the linear dependence between the MAPE and the database size decreased as the percentage strain analyzed increased. This suggests that there is a relationship between the shape of the stress-strain curve and the sE_{max} since the more information of the shape is provided, a more accurate decision can be performed even when the database is formed by only 2 curves. However, due to the high variability in shapes and sE_{max} this does not happen for all curves as can be observed from the high standard deviation at this database size.

Discussion The accuracy results for the *leave-one-out* test with the complete set of 97 curves showed that having a wide range of possible sE_{max}values for each curve and that the selection of this value depended on the similarity of the stress-strain curves, can reduce the absolute percentage error in the prediction. From the *leave-one-out test* and the *complementary curves* test using databases constructed with randomly chosen curves, the MAPE plots showed that it is necessary to have around 30 curves or higher in the database to decrease the standard deviation considerably with respect to the left extremes of the plots no matter the number of curves for which the prediction was done. In the case of the *leave-one-out test* the number being the same as the database size and for the *complementary curves* test the number would decrease as the database size increased. It could also be observed that there was no linear dependence between the MAPE and the database size in the *leave-one-out test* and a weak dependence in the *complementary curves* test which obeyed to the fact of having each time fewer number of curves with a higher number of different shapes to which the match could be done.

Furthermore, the accuracy of the prediction was consistent for a similar database size between both tests, i.e. whether the prediction was performed once for one curve, as observed from the MAPE values of the right end of the MAPE plot of the *complementary curves* test, or if it was performed many times for a group of curves as observed from the right end of the MAPE plot of the *leave-one-out* test. Moreover, for both analyses it can be observed that the behavior of the error was similar for the three strain percentages such that using a fraction of the stress-strain curve up to 5% proved more convenient since the prediction can be carried out for a higher number of curves without exceeding the sE_{max}.

A.3.5 *Interspecies application*

A sensitivity analysis was performed for the comparison between using up to 2% or 3% strain of the stress-strain curve. The statistical methods used for this analysis were the Skillings-Mack test and multiple imputation followed by either a related samples Wilcoxon signed rank test or a paired t-test. The two approaches yielded the same results with respect to the significance of each pairwise comparison, except for one case: between the minimum MAPE of both strain percentages for the Norm-UTS-FStrain case.

B FIGURES

FIGURE CAPTIONS

FIGURE 1. Mullin's effect during the first loading cycles of the porcine digital flexor tendon.

FIGURE 2. Mechanical components of the tendon loading device. a) Eccentric wheel: controls the vertical displacement of the upper clamp. b) Clamps and chamber: hold the explant in place during the loading tests.

FIGURE 3. Electronics of the tendon loading device: a) amplifier, b) power Supply, c) EPOS Maxon motor controler, d) Maxon motor, e) force sensor.

FIGURE 4. EPOS Interface: used to control the RPM of the DC motor of the tendon loading device.

FIGURE 5. Front panel of Labview interface: used to monitor the acquisition of the load-displacement data.

FIGURE 6. Part 1 of the block diagram. This part is involved in receiving the voltages of the displacement and force sensores and displaying the load-displacement graph.

FIGURE 7. Part 2 of the block diagram. This part was involved in gathering the last 5 data points before a peak of the load-displacement curve, once a peak was detected.

FIGURE 8. Part 3 of the block diagram. This part was involved in using the previously gathered data points for the calculation of the elastic stiffness of each cycle during the fatigue loading tests. This part is also capable of the following: 1) saving the stiffness of the cycle at which it is decided to start the analysis of the degradation of the stiffness and 2) Establish a critical stiffness as a percentage of the stiffness recorded in 1) and 3) detect and alarm when this critical value has been passed.

FIGURE 9. Work environment

FIGURE 10. Washing and disinfection.

FIGURE 11. Deskinning of the leg

FIGURE 12. Cutting of the tendon into explants

FIGURE 13. Storage of the explants

FIGURE 14. Loading of the explant. a) Explant loading equipment and b) tendon explant clamped with aid of sand paper in initial position before failure test.

FIGURE 15. Slippage detection: usage of a) Indian blue ink to b) mark the explant.

FIGURE 16. Fitting of the explant's failure curve with a sum of Gaussian curves.

FIGURE 17. Fitting the 97 failure curves.

FIGURE 18. Finding the minimum RMSE error between the sample's stress-strain curve and the 97 failure curves.

FIGURE 19. Leave-one-out principle: one failure curve is left out of the database and used as experimental sample while the rest are used for the shape comparison with the sample.

FIGURE 20. Diagram of the leave-one-out test principle and the comparison between the sample and the rest of the curves in the database.

FIGURE 22. Crimp pattern differences between the a) SDFT and b) DDFT (V.L.C. Feitosa 2006).

FIGURE 23. MAPE ± SD (%) between the real sE_{max} and a fixed strain value used as a prediction of the former.

FIGURE 24. RMSE (%) value of the prediction of all curve's strain at the maximum Young's Modulus using the same strain value in all predictions.

FIGURE 25. Influence of the smoothing span in the extrapolation curve. The a) improvement in the extrapolation curve for some curves when comparing two different spans was counterbalanced with the b) deterioration in the extrapolation curve of other curves when using the same spans.

FIGURE 26. Distribution of the absolute percentage error for the leave-one-out test using a shape-based comparison method for the prediction of sE_{max}.

FIGURE 27. MAPE ± SD (%) at each of the different database sizes. The leave-one-out test was used for the evaluation of the shape-based comparison method for the prediction of $sE_{max}$of the porcine tendon explants. Note: Only each 5 database sizes were plotted for clarity.

FIGURE 28. MAPE ± SD (%) of the test where the curves complementary to those randomnly chosen for the construction of the database were used as samples for estimation of their sE_{max}.

FIGURE 29. MAPE ± SD (%) of the prediction of sE_{max} of the 97 porcine tendon explants' stress-strain curves by using the shape-based comparison method in its variant that considers the mean of the sE_{max} of the n closest curves.

FIGURE 30. Normalization of the pigs' and horses' stress-strain curves w.r.t. the mean UTS and mean failure strain and w.r.t. the mean UTS and mean sEmax of the respective species.

FIGURE 31. Mean ± SD of the MAPE (%) at each of the different database sizes (Each of the 10 iterations results in a MAPE value). The horse curves were compared to the pig curves in order to evaluate the shape-based comparison method for the prediction of $sE_{max}$of tendon explants of different species. Note: Only each 5 database sizes were plotted for clarity. a) No normalization, b) Normalization w.r.t. UTS and sE_{max} and c) Normalization w.r.t. UTS and failure strain.

B.1 *Materials*

B.1.1 *Experimental samples*

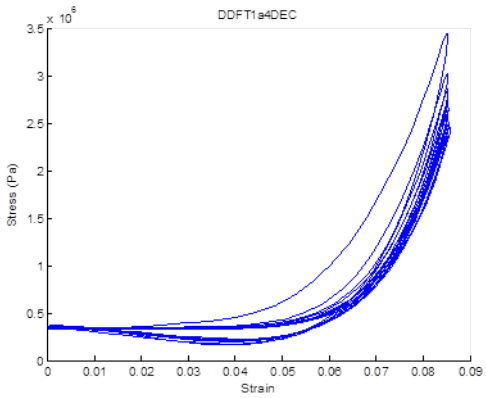

Figure 1

B.1.2 *Hardware: Mechanical*

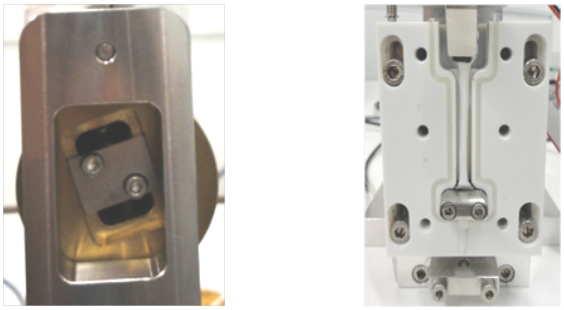

(a) **(b)**

Figure 2

B.1.3 *Hardware: Electronics*

(a) **(b)** **(c)**

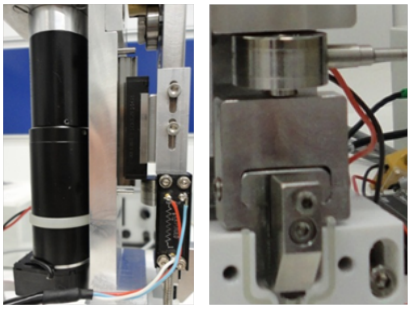

(d) **(e)**

Figure 3

B.1.4 *Software*

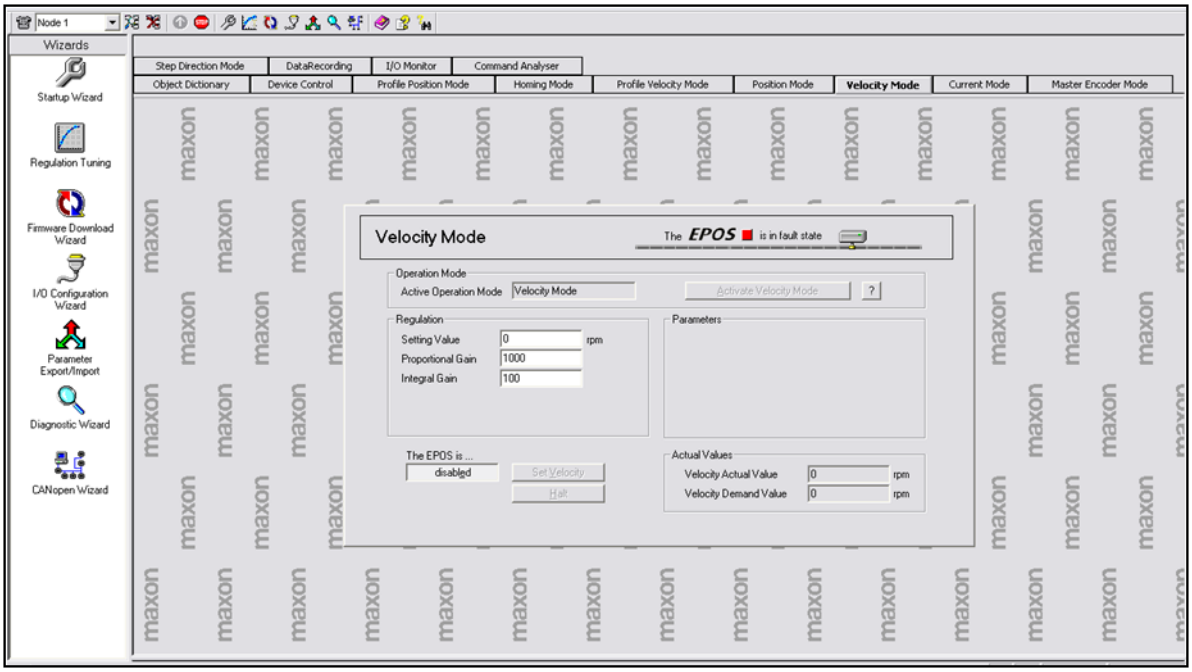

Figure 4

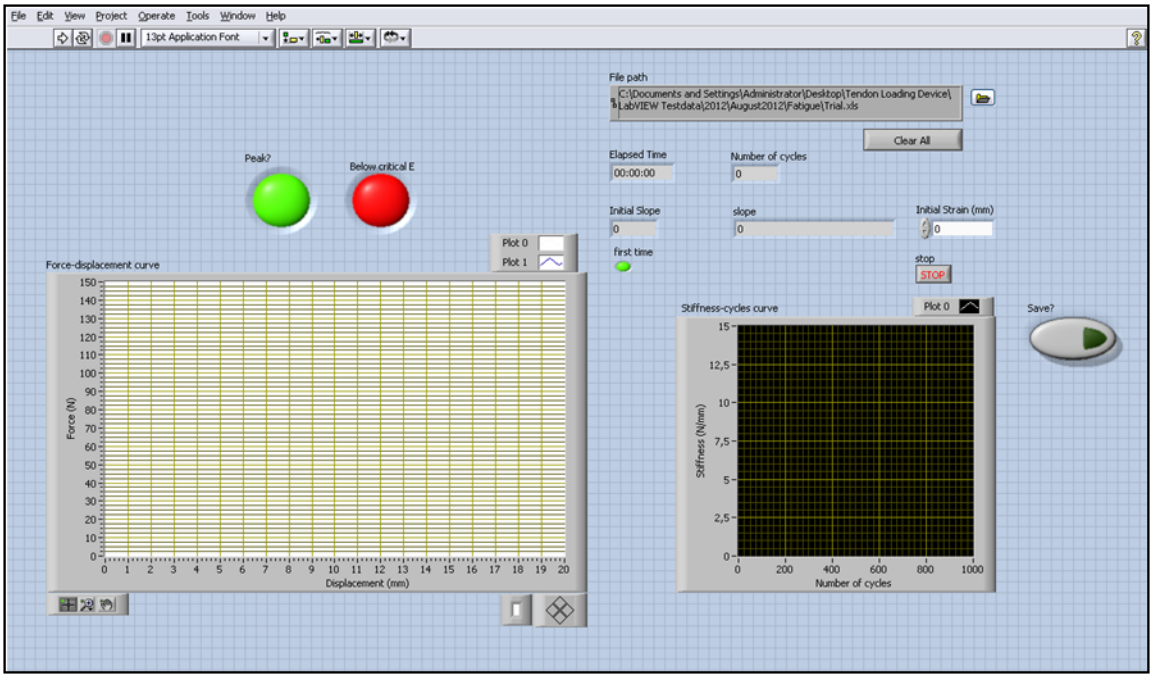

Figure 5

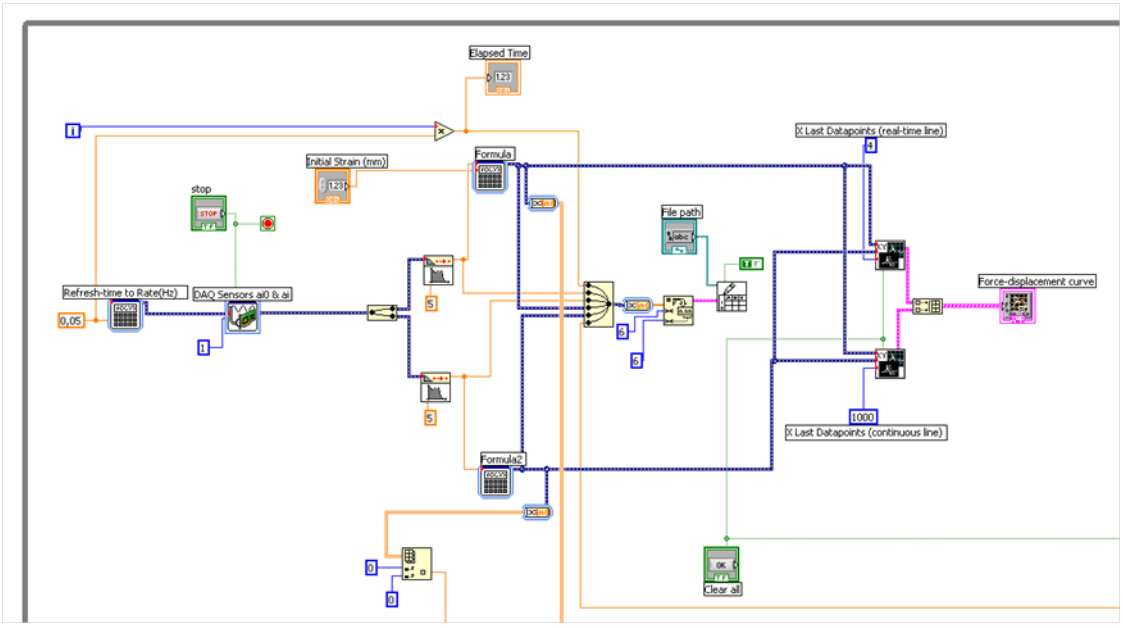

Figure 6

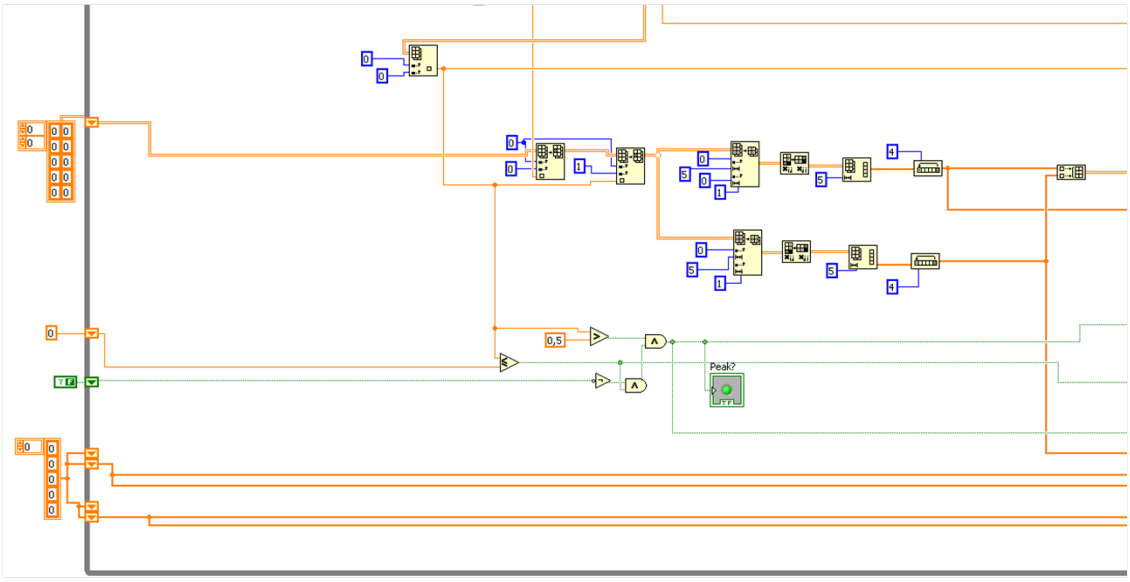

Figure 7

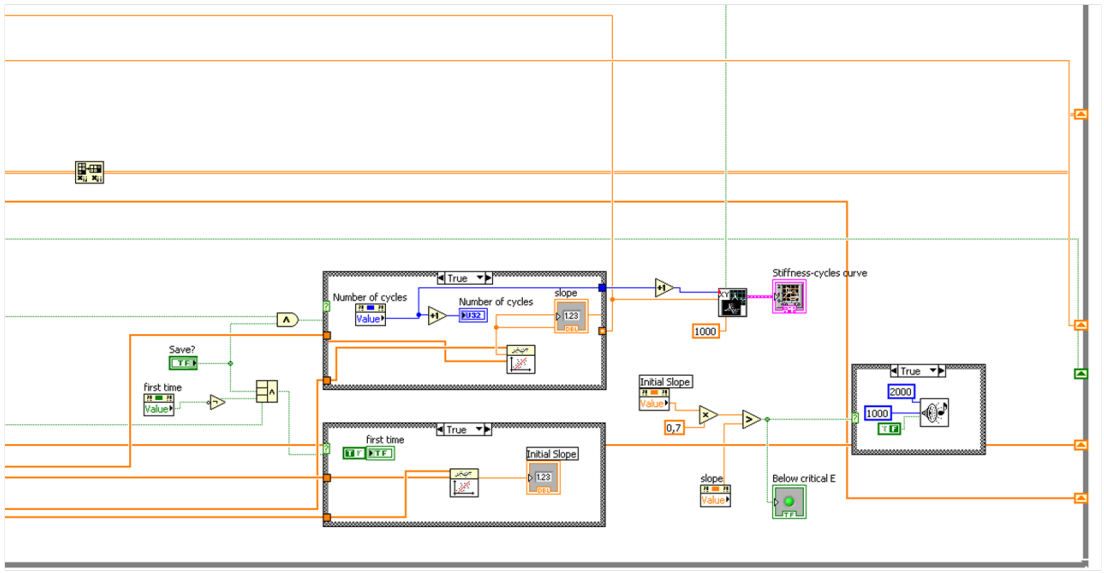

Figure 8

B.2 *Methods*

B.2.1 *Tendon explants isolation*

FIGURE

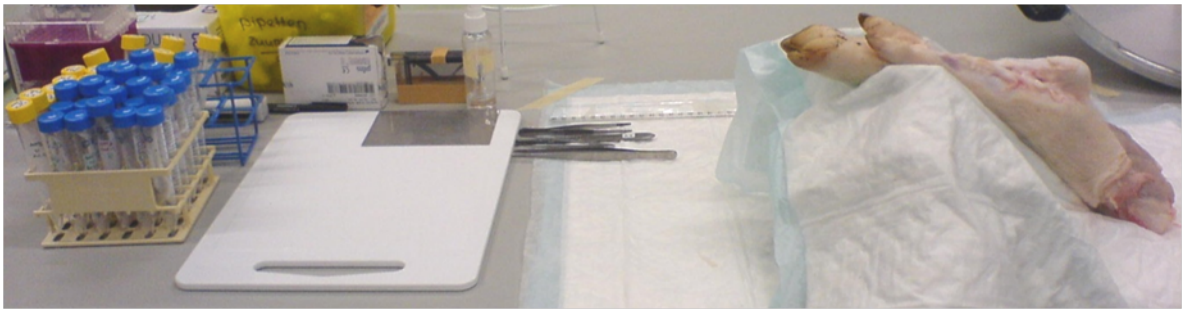

Figure 9

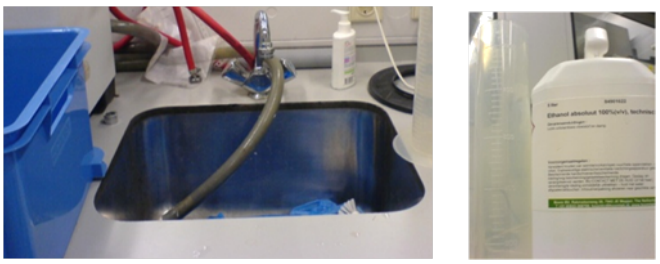

(a) **(b)**

Figure 10

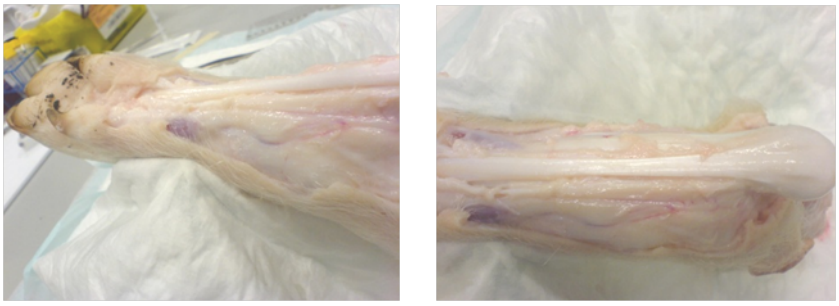

(a) Antero-lateral view of the porcine SDFT

(b) Superior view of the porcine SDFT

Figure 11

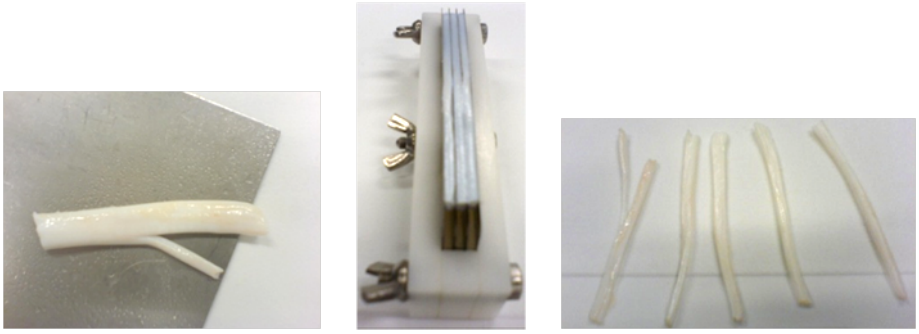

(a) Deep Digital Flexor Tendon (DDFT) with adjacent X tendon

(b) 'Spaghetti cutter'

(c) Explants from the isolated piece of tendon

Figure 12

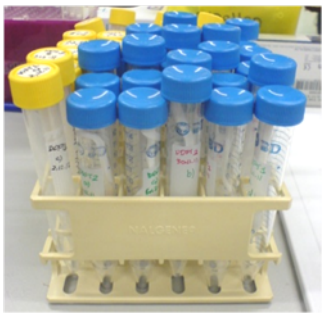

Figure 13

B.2.2 *Failure tests*

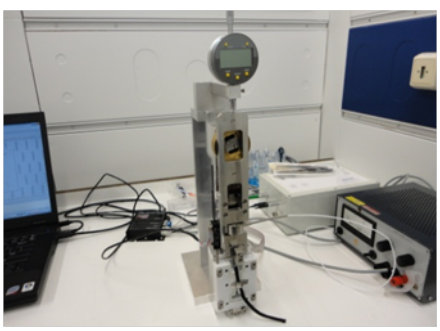

(a)

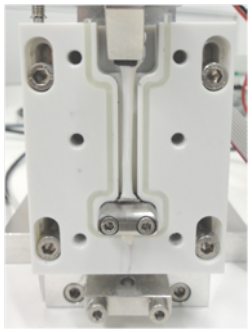

(b)

Figure 14

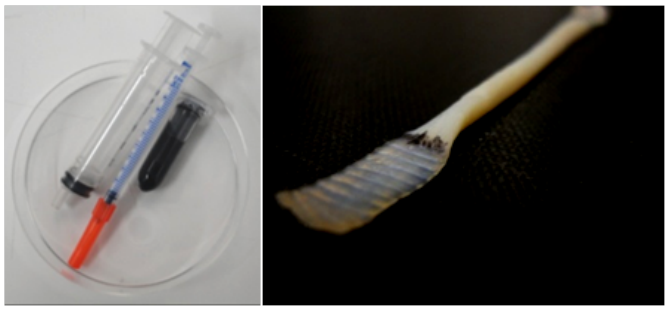

Figure 15

B.2.3 *Comparison of different approaches to predict the elastic limit*

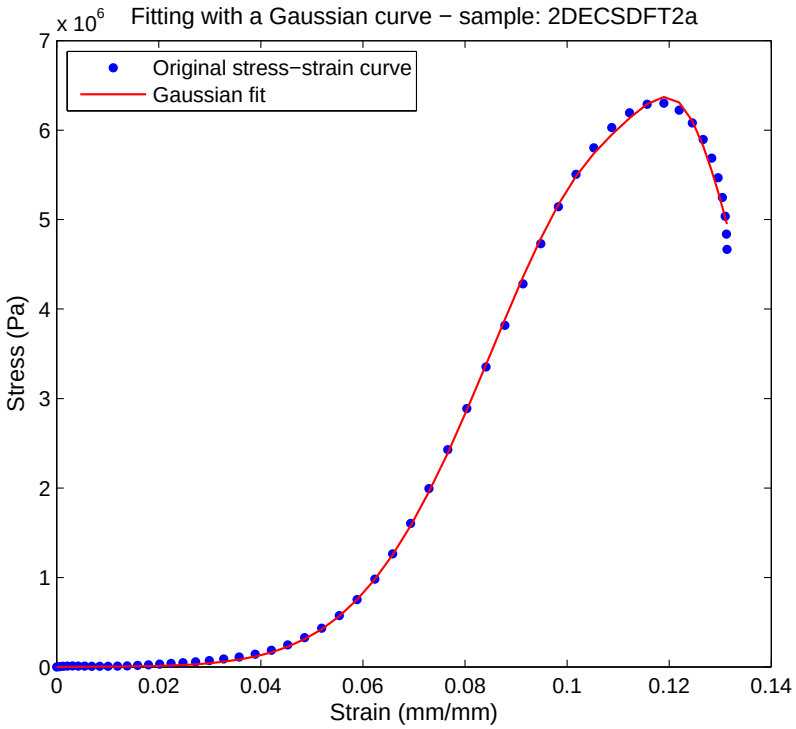

Figure 16

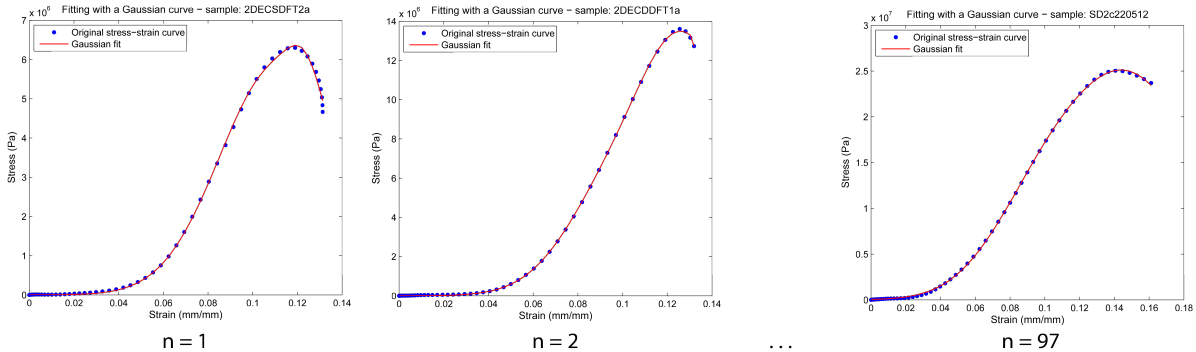

Figure 17

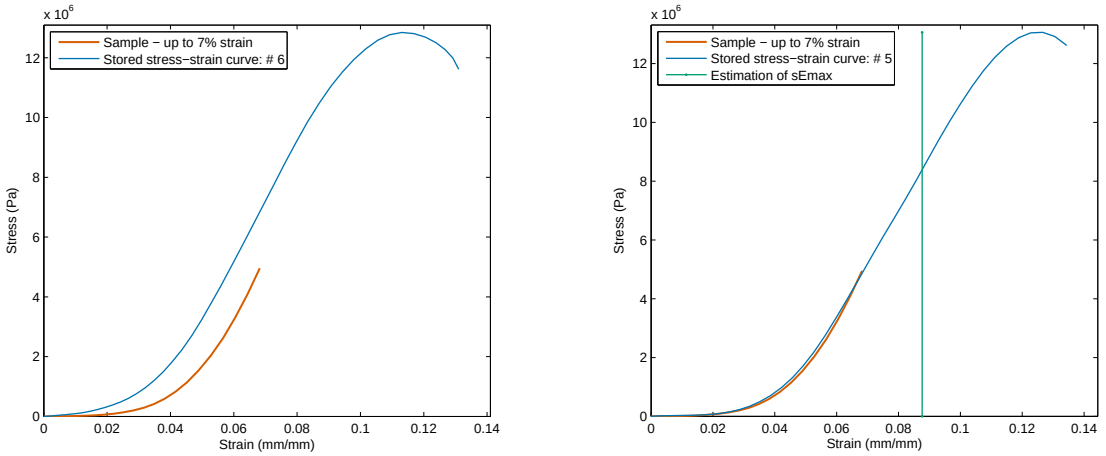

(a) Sample's stress-strain curve compared to same fraction of failure curve #6

(b) In this example, the minimum RMSE error was found when compared to failure curve #5

Figure 18

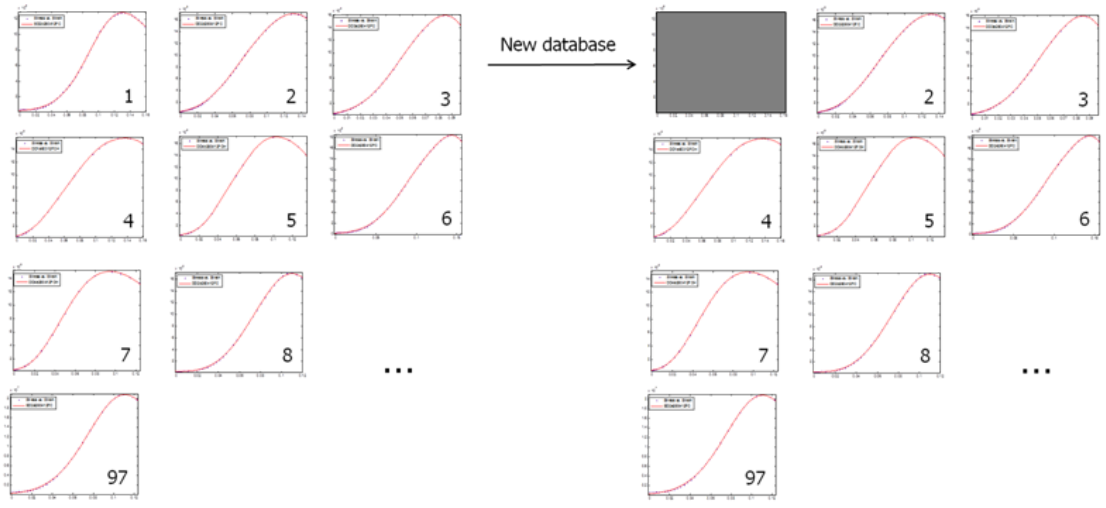

Figure 19

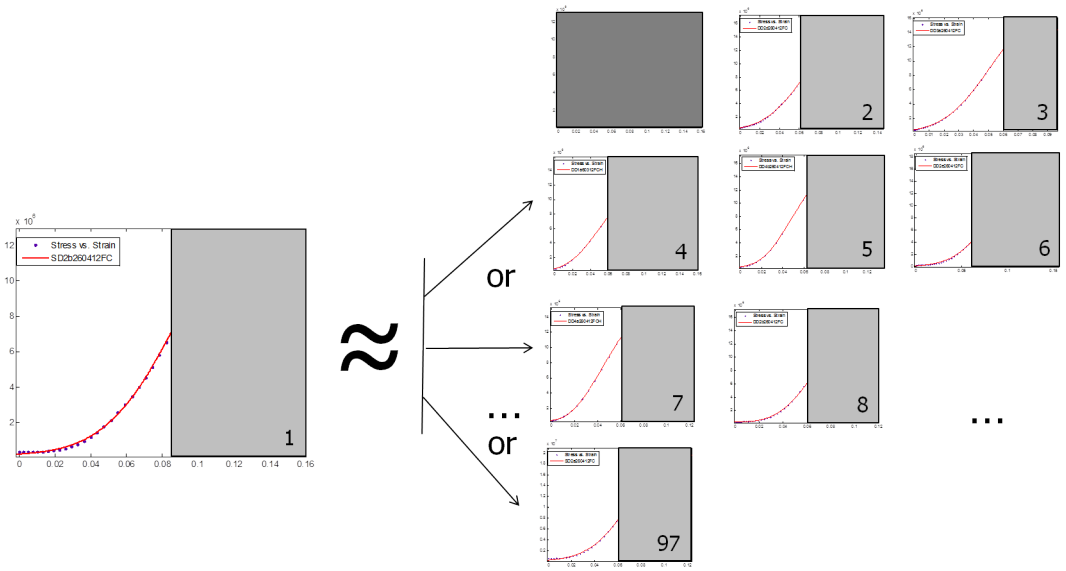

Figure 20

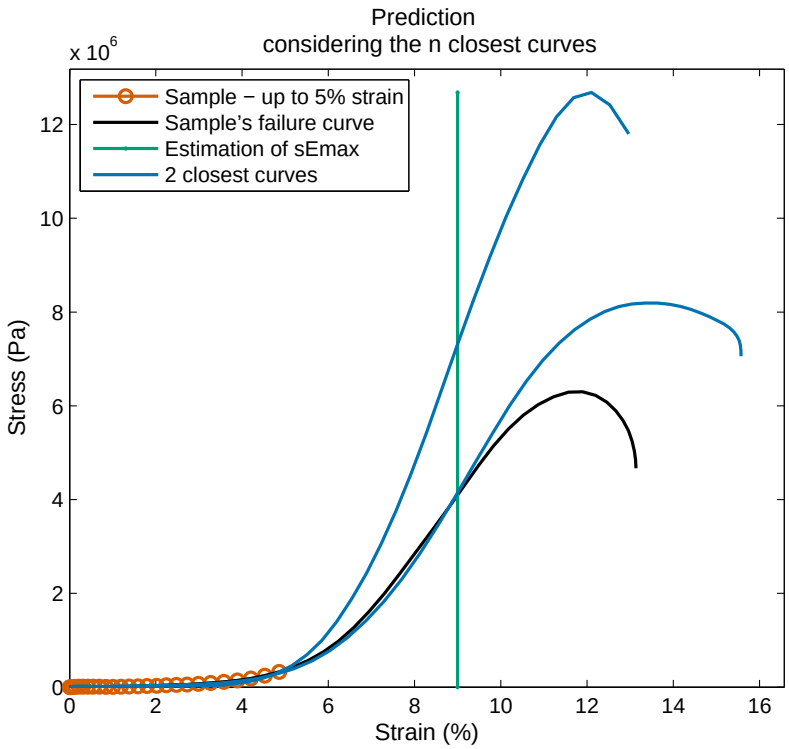

Figure 21

B.3 *Results*

B.3.1 *Failure tests*

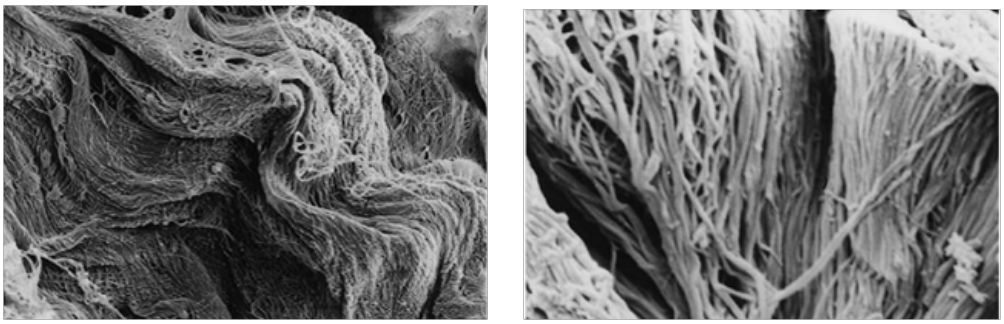

(a) **(b)**

Figure 22

B.3.2 *Single strain value used as an estimation of sEmax*

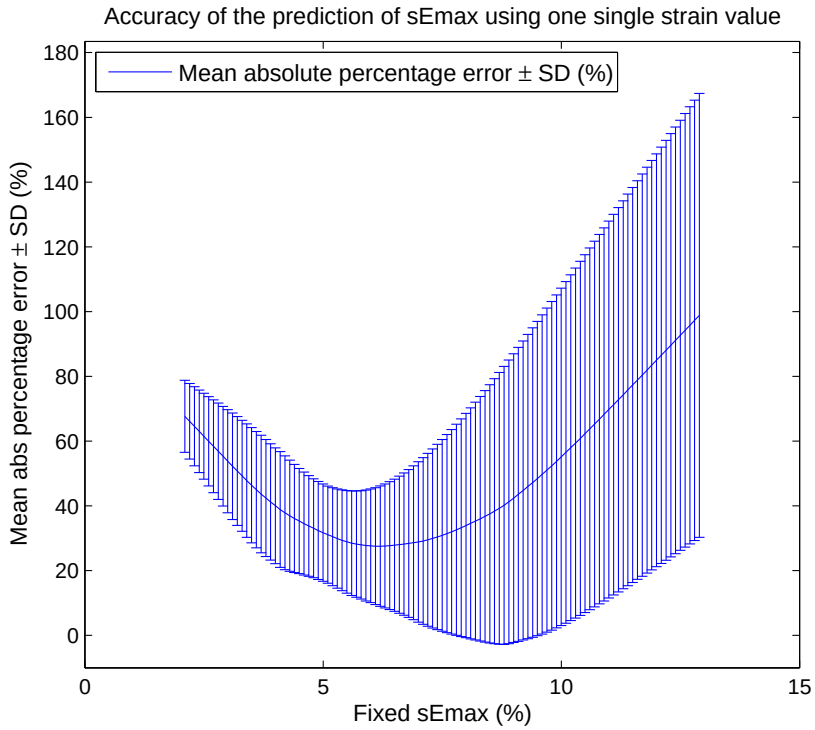

Figure 23

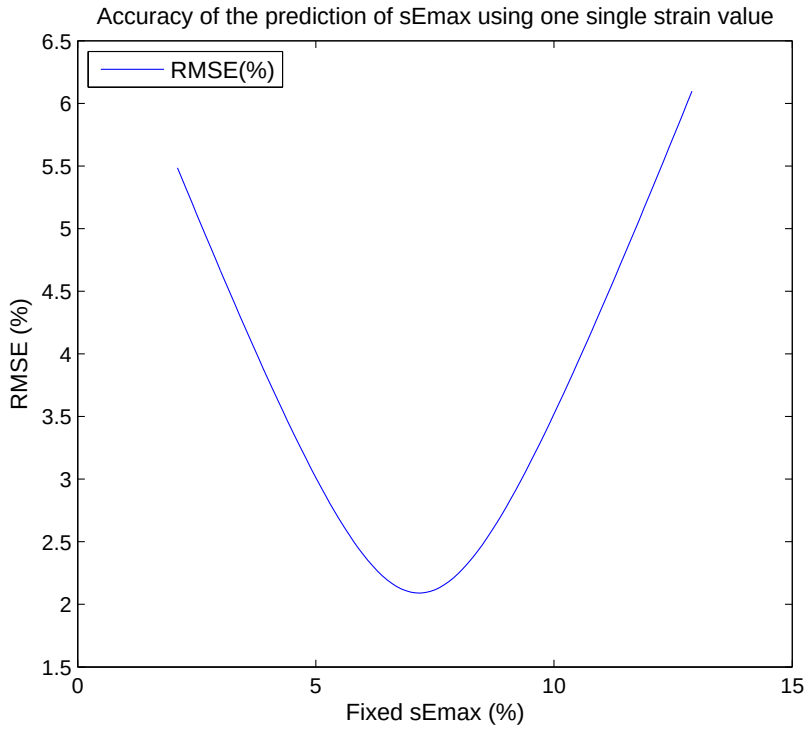
Accuracy of the prediction of sEmax using one single strain value
RMSE(%)
RMSE (%)
Fixed sEmax (%)
6.5
6
5.5
5
4.5
4
3.5
3
2.5
2
1.5
0
5
10
15

Figure 24

B.3.3 *Extrapolation method*

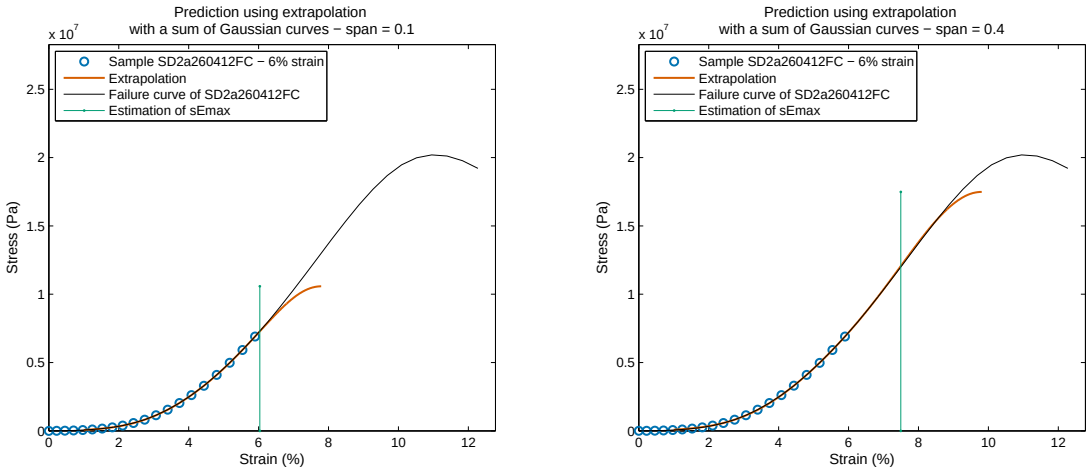

(a)

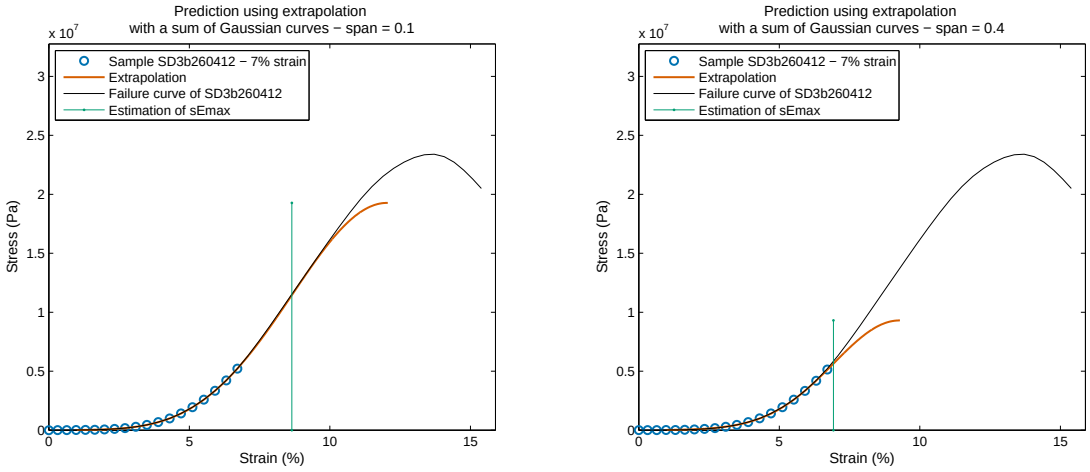

(b)

Figure 25

B.3.4 *Shape-based comparison method*

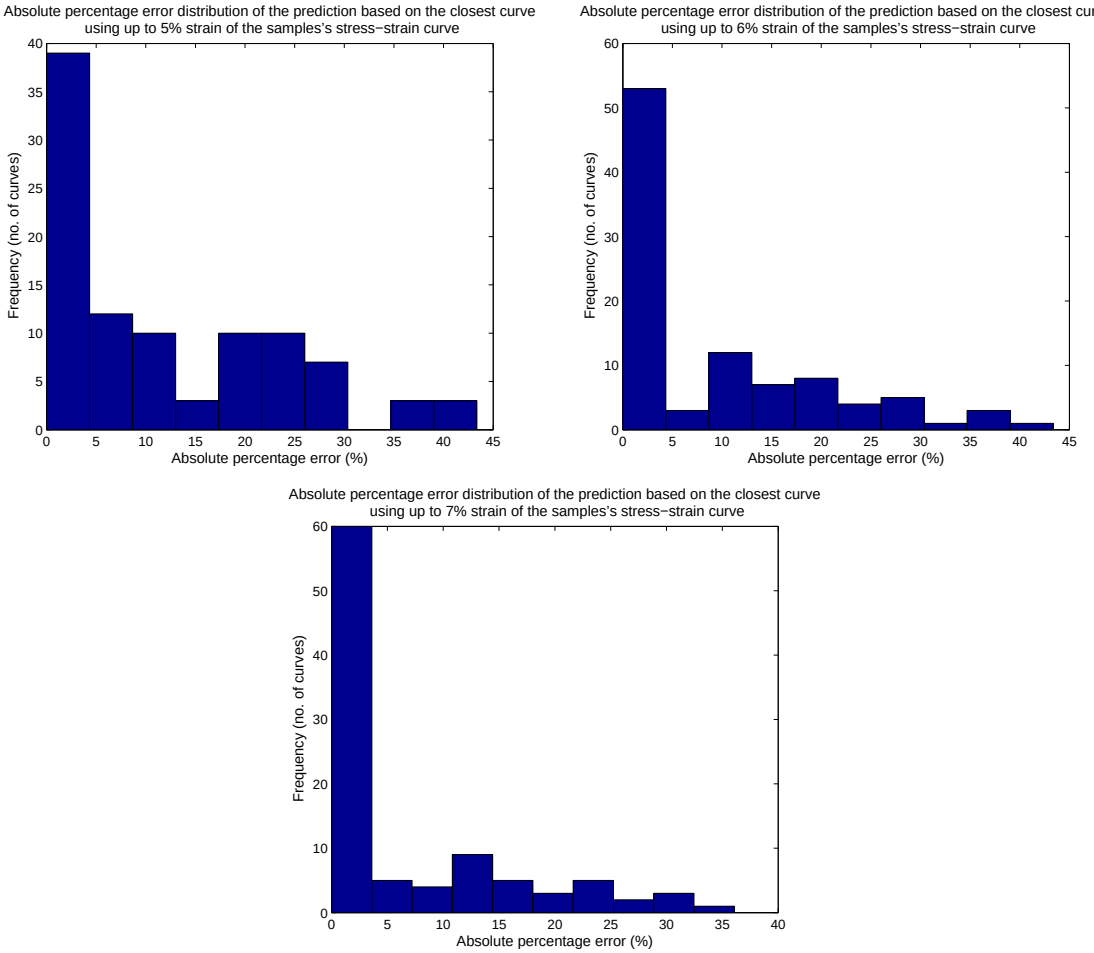

Figure 26

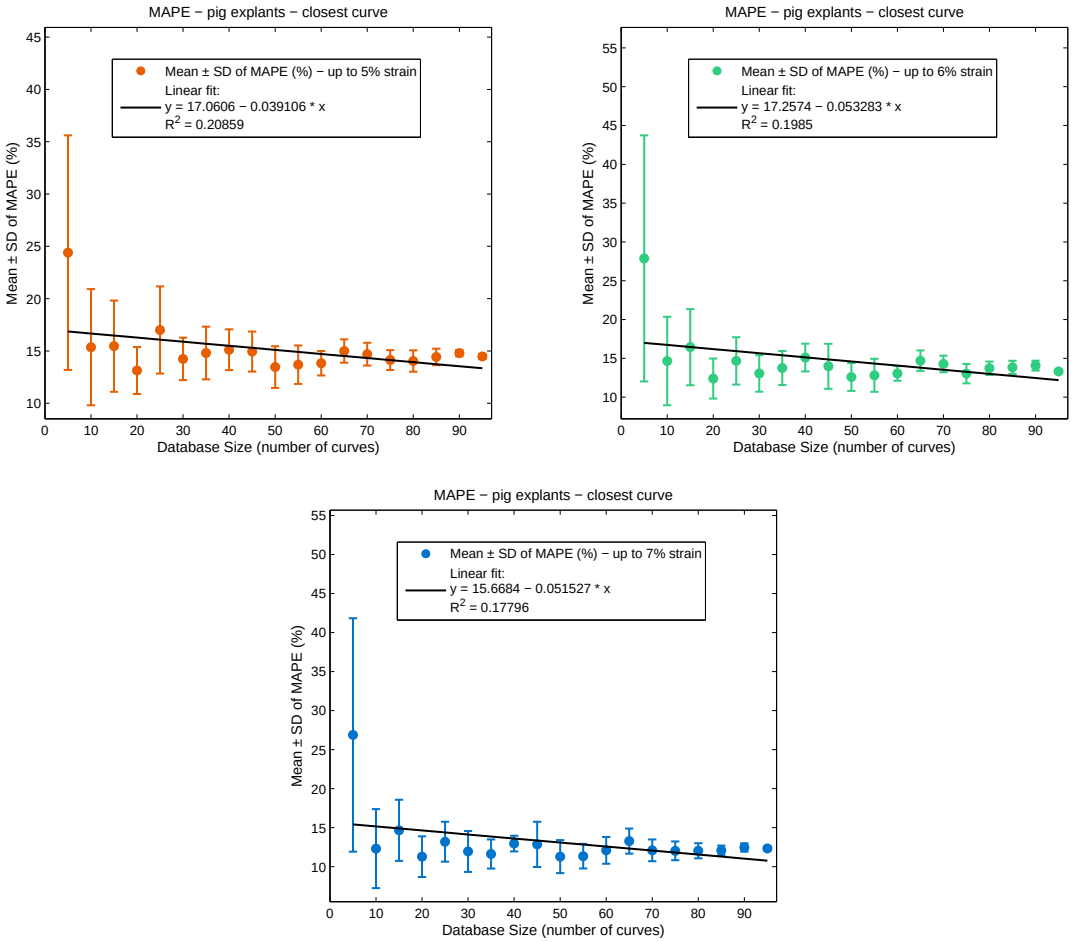
MAPE − pig explants − closest curve
Mean ± SD of MAPE (%) − up to 5% strain
Linear fit:
y = 17.0606 − 0.039106 * x
R2 = 0.20859
Mean ± SD of MAPE (%)
Database Size (number of curves)
MAPE − pig explants − closest curve
Mean ± SD of MAPE (%) − up to 6% strain
Linear fit:
y = 17.2574 − 0.053283 * x
R2 = 0.1985
Mean ± SD of MAPE (%)
Database Size (number of curves)
MAPE − pig explants − closest curve
Mean ± SD of MAPE (%) − up to 7% strain
Linear fit:
y = 15.6684 − 0.051527 * x
R2 = 0.17796
Mean ± SD of MAPE (%)
Database Size (number of curves)

Figure 27

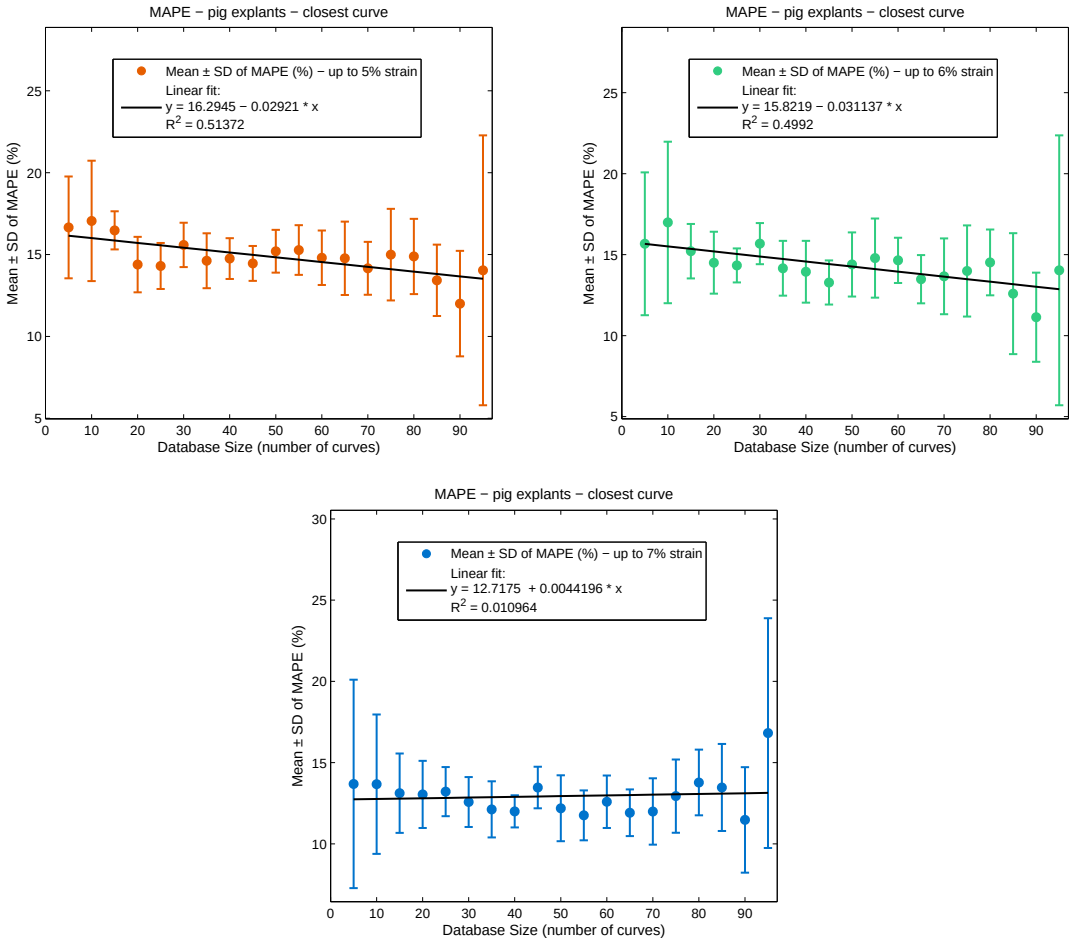
MAPE − pig explants − closest curve
Mean ± SD of MAPE (%) − up to 5% strain
Linear fit:
y = 16.2945 − 0.02921 * x
R2 = 0.51372
Mean ± SD of MAPE (%)
Database Size (number of curves)
MAPE − pig explants − closest curve
Mean ± SD of MAPE (%) − up to 6% strain
Linear fit:
y = 15.8219 − 0.031137 * x
R2 = 0.4992
Mean ± SD of MAPE (%)
Database Size (number of curves)
MAPE − pig explants − closest curve
Mean ± SD of MAPE (%) − up to 7% strain
Linear fit:
y = 12.7175 + 0.0044196 * x
R2 = 0.010964
Mean ± SD of MAPE (%)
Database Size (number of curves)

Figure 28

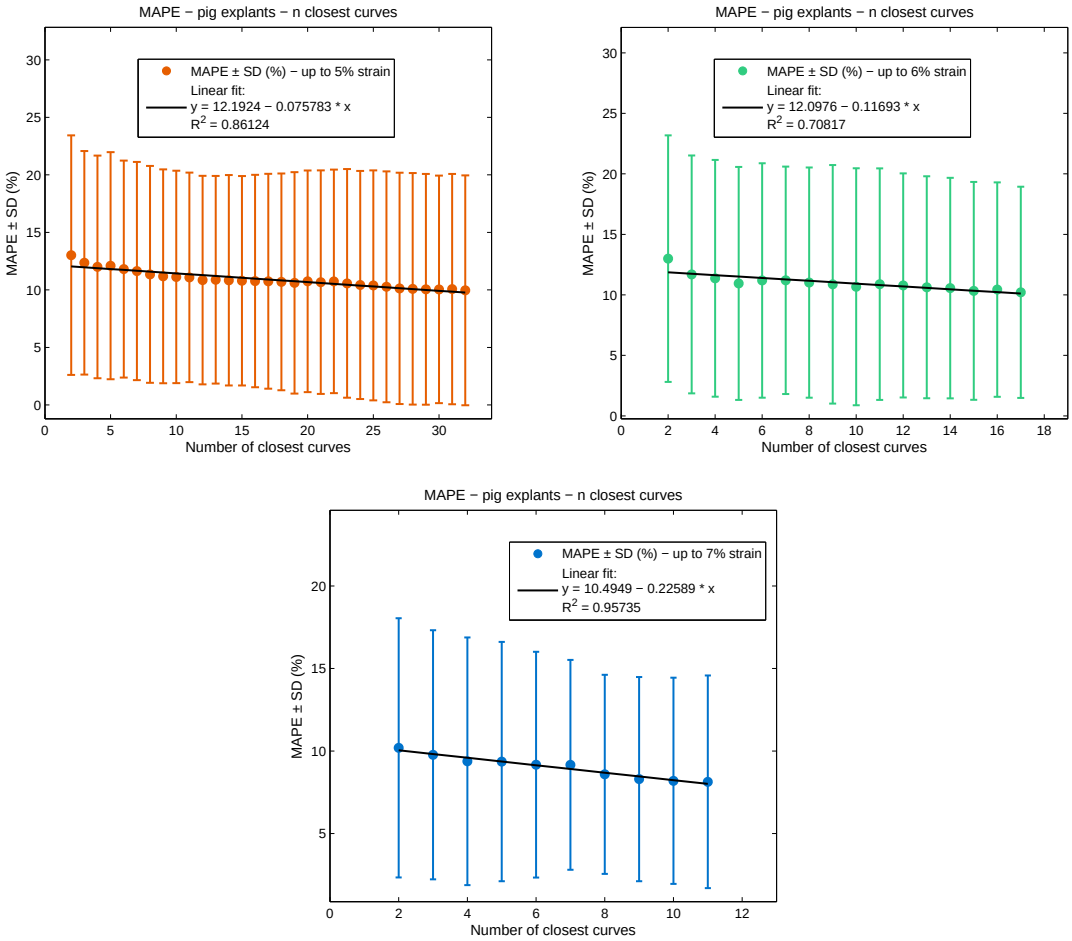
MAPE − pig explants − n closest curves
MAPE ± SD (%) − up to 5% strain
Linear fit:
y = 12.1924 − 0.075783 * x
R2 = 0.86124
MAPE ± SD (%)
Number of closest curves
MAPE − pig explants − n closest curves
MAPE ± SD (%) − up to 6% strain
Linear fit:
y = 12.0976 − 0.11693 * x
R2 = 0.70817
MAPE ± SD (%)
Number of closest curves
MAPE − pig explants − n closest curves
MAPE ± SD (%) − up to 7% strain
Linear fit:
y = 10.4949 − 0.22589 * x
R2 = 0.95735
MAPE ± SD (%)
Number of closest curves

Figure 29:

B.3.5 *Interspecies application*

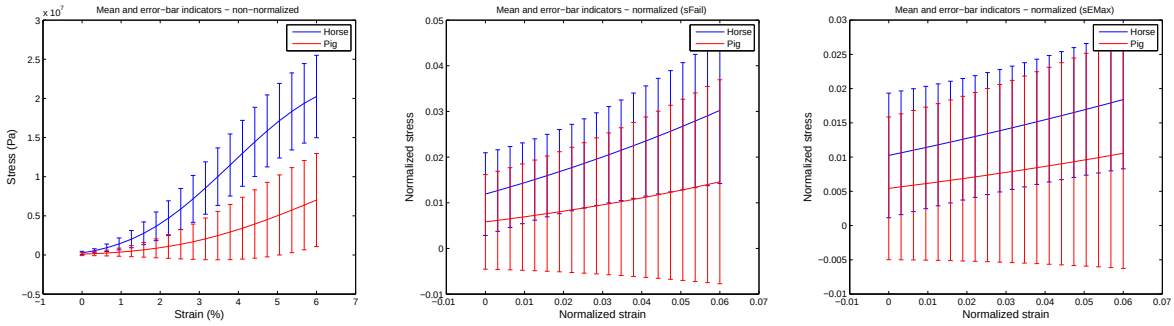

(a)

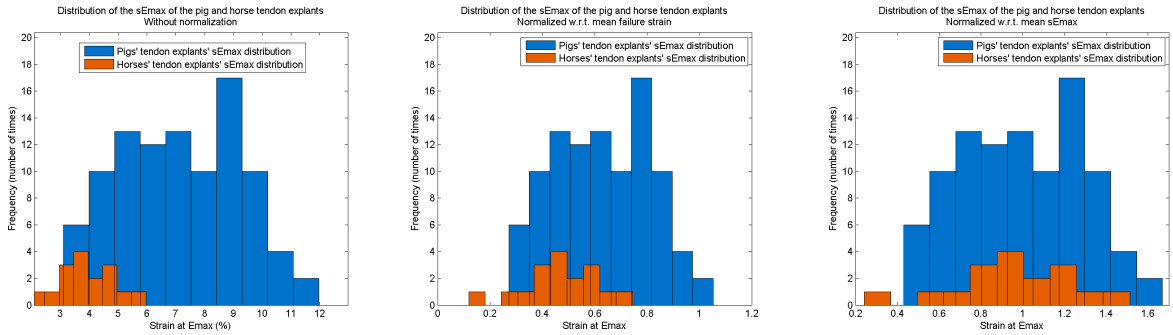

(b)

Figure 30

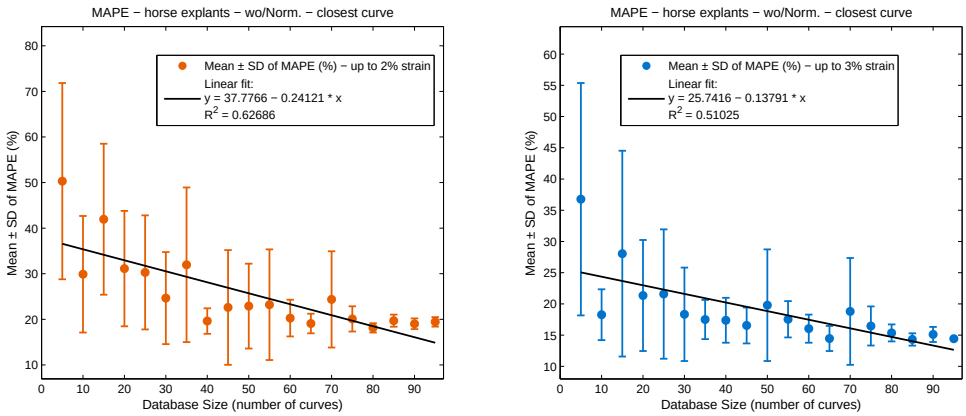

(a)

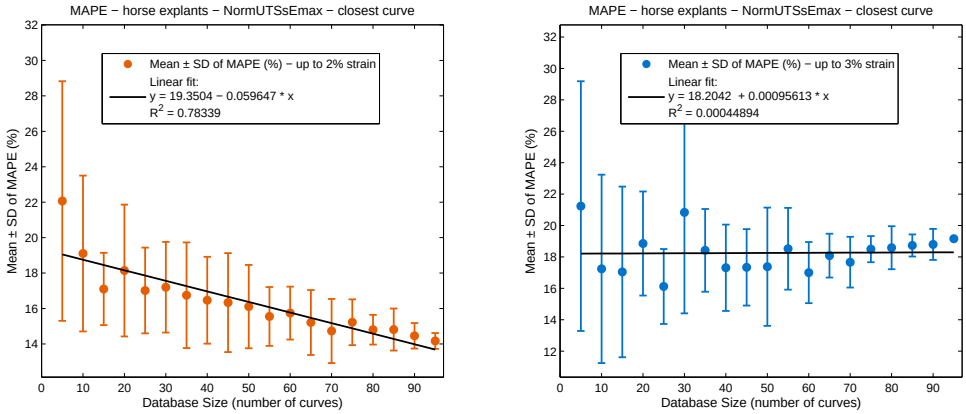

(b)

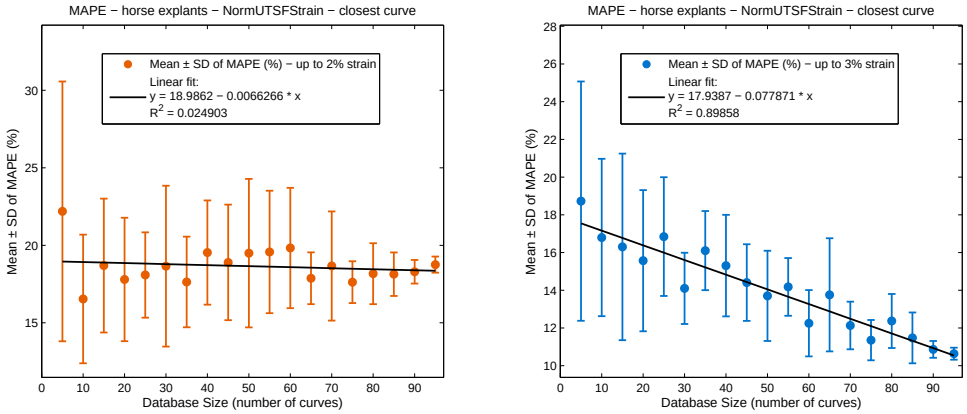

(c)

Figure 31:

C TABLES

TABLE CAPTIONS

TABLE 1. Connections of the EPOS Maxom motor controler.

TABLE 2. Electronic components' characteristics.

TABLE 3. Goodness of fit (based on the R^2) to the 97 failure curves of the porcine flexor tendon explants for different types of curves.

TABLE 4. Failure load (N), UTS (MPa) and CSA (m^2) of the pig's superficial and deep digital flexor tendons (mean ± SD). * represents significant differences ($p < 0.05$).

TABLE 5. Strain at the end of the toe region, strain at E_{max}, yield strain and failure strain of the pig's superficial and deep digital flexor tendons (mean ± SD). * represents significant differences ($p < 0.05$).

TABLE 6. Maximum Young's Modulus (E_{max}), Elastic Modulus and Young's Modulus of the quasi-linear region of the pig's superficial and deep digital flexor tendons (mean ± SD). * represents significant differences ($p < 0.05$).

TABLE 7. Failure load (N), UTS (MPa) and CSA (m^2) of the horse's SDFTs (mean ± SD). * represents significant differences ($p < 0.05$).

TABLE 8. Strain at the end of the toe region, strain at E_{max}, yield strain and failure strain of the horse's SDFTs (mean ± SD). * represents significant differences ($p <0.05$).

TABLE 9. Maximum Young's Modulus (E_{max}), Elastic Modulus and Young's Modulus of the quasi-linear region of the horse's SDFTs (mean ± SD). * represents significant differences ($p < 0.05$).

TABLE 10. MAPE ± SD (%) (first row) and RMSE (%) (second row) for the prediction of sE_{max} using an extrapolation curve. Different orders of gaussian, polynomial and fourier series were tested. All the results correspond to a smoothing span of 0.2 and to the mean failure strain as the end value of the extrapolation vector.

TABLE 11. Extrapolation performance for the different orders of gaussian, polynomial and fourier series used: 1) percentage of predictions that could be carried out (P), 2) percentage of overpredictions (!) out of those in 1) and their MAPE ± SD (%) and 3) the percentage of cases in which the extrapolation curve became negative (-) out of those in 1).

TABLE 12. APE ± SD (%) and RMSE (%) of the prediction of sE_{max} with shape-based comparison method in its two approaches. C stands for closest-curve approach and N-C stands for N-closest curves approach, where N corresponds to that at which the minimum MAPE (%) was found for each strain percentage.

TABLE 13. MAPE ± SD (%) and RMSE (%) of the sE_{max} prediction of the horses' stress-strain curves without normalization of the two species loading curves. The results shown for the n closest curves method belong to n = 2.

TABLE 14. MAPE ± SD (%) and RMSE (%) of the sE_{max} prediction of the horses' stress-strain curves with normalization of the two species loading curves w.r.t. their respective UTS and sE_{max}. The results shown for the n closest curves method belong to that n at which the minimum MAPE was found for each strain percentage: N = 28 for 2% and N = 29 for 3%.

TABLE 15. MAPE ± SD (%) and RMSE (%) of the sE_{max} prediction of the horses' stress-strain curves with normalization of the two species loading curves w.r.t. their respective UTS and failure strain. The results shown for the n closest curves method belong to that n at which the minimum MAPE was found for each strain percentage: N = 13 for 2% and N = 25 for 3%.

C.1 *Materials*

Table 1

Connection	Function
J1 - Power Supply	Receives the voltage from the power supply
J2 - Motor	Supplies the motor with the voltage
J3 - Encoder	Controls the position of the motor

Table 2

Component	Characteristic
Motor	RE 35, Ø35 mm
	Graphite Brushes
	90 Watt
Force sensor	−0.0072 mV/V (minimum output voltage/excitation voltage without fitting parts)

C.2 *Methods*

Table 3

Order	Gauss		Polynomial	Fourier series
1	0.99727			
2	0.99948	0.99976		0.99971
3	0.99942		0.99318	0.99991
4			0.99912	0.99997
5			0.99969	
6			0.99988	
7			0.99993	
8			0.99996	

C.3 *Results*

C.3.1 *Failure tests*

Table 4

	SDFT	DDFT
Failure load (N)	71.48 ± 25.86	80.86 ± 24.33
UTS (MPa)	19.29 ± 9.07	16.23 ± 5.22
CSA (m^2)*	$4.08E^{-06} \pm 1.16E^{-06}$	$5.12E^{-06} \pm 1.07E^{-06}$

Table 5

	SDFT	DDFT
Strain End Toe Region (%)*	6 ± 2	5 ± 2
Strain at E_{max} (%)*	8 ± 2	7 ± 2
Yield strain (%)*	10 ± 2	8 ± 3
Failure Strain (%)*	12 ± 2	11 ± 3

Table 6

	SDFT	DDFT
$E_{max}(GPa)$	0.32 ± 0.16	0.28 ± 0.09
Elastic Modulus (GPa)	0.29 ± 0.15	0.25 ± 0.08
Young's Modulus of the quasi-linear region (GPa)	0.29 ± 0.14	0.25 ± 0.08

Table 7

	Frison
Failure load (N)	102.16 ± 40.28
UTS (MPa)	23.81 ± 6.01
CSA (m^2)	$4.43E^{-06} \pm 1.79E^{-06}$

Table 8

	Frison
Strain End Toe Region (%)	2 ± 1
Strain at E_{max} (%)	4 ± 1
Yield strain (%)	5 ± 1
Failure Strain (%)	8 ± 2

Table 9

	Frison
$E_{max}(GPa)$	0.52 ± 0.11
Elastic Modulus (GPa)	0.47 ± 0.10
Young's Modulus of the quasi-linear region (GPa)	0.47 ± 0.10

C.3.2 *Extrapolation method*

Table 10

Extrapolation	5%	6%	7%
Gauss 2	27.48 ± 13.22	24.12 ± 11.00	18.13 ± 10.10
	2.51	2.33	1.92
Gauss 3	31.87 ± 15.00	27.76 ± 13.94	19.75 ± 11.76
	2.98	2.85	2.11
Poly 4	22.45 ± 14.47	20.48 ± 15.82	14.48 ± 11.97
	1.96	1.80	1.51
Poly 5	18.81 ± 11.57	14.27 ± 8.49	13.54 ± 8.46
	1.82	1.40	1.44
Poly 6	30.43 ± 17.55	19.32 ± 10.43	18.74 ± 11.13
	2.79	1.99	1.97
Poly 7	38.75 ± 21.48	27.29 ± 17.03	17.28 ± 9.28
	3.54	2.77	1.93
Poly 8	32.12 ± 15.18	28.39 ± 16.37	16.08 ± 9.99
	3.02	2.68	1.83
Fourier 2	19.74 ± 12.71	13.62 ± 8.18	13.10 ± 9.89
	1.90	1.33	1.38
Fourier 3	30.59 ± 17.07	19.29 ± 11.85	16.62 ± 11.83
	2.86	2.04	1.80
Fourier 4	33.52 ± 17.26	24.93 ± 14.91	16.24 ± 9.29
	3.22	2.56	1.83

Table 11

Extrapolation		5%	6%	7%
Gauss 2	P:	88.61	92.31	86.79
	(!):	4.29	8.33	8.70
		4.51 ± 2.76	21.26 ± 12.29	8.94 ± 11.93
	(-):	4.29	1.67	6.52
Gauss 3	P:	84.81	81.54	92.45
	(!):	10.45	5.66	4.08
		18.46 ± 14.40	16.98 ± 8.06	19.14 ± 13.16
	(-):	10.45	7.55	8.16
Poly 4	P:	36.71	43.08	45.28
	(!):	37.93	46.43	58.33
		26.06 ± 16.32	28.99 ± 17.04	16.20 ± 13.15
	(-):	55.17	10.71	0.00
Poly 5	P:	51.90	69.23	66.04
	(!):	17.07	26.67	31.43
		13.72 ± 11.35	8.22 ± 6.54	11.79 ± 8.29
	(-):	70.73	53.33	20.00
Poly 6	P:	72.15	75.38	64.15
	(!):	8.77	10.20	17.65
		46.79 ± 42.91	4.21 ± 1.25	25.00 ± 15.53
	(-):	87.72	73.47	35.29
Poly 7	P:	46.84	40.00	45.28
	(!):	10.81	19.23	16.67
		80.28 ± 33.80	37.64 ± 29.32	17.48 ± 7.92
	(-):	83.78	73.08	50.00
Poly 8	P:	58.23	58.46	58.49
	(!):	6.52	10.53	6.45
		38.34 ± 33.81	62.20 ± 20.11	2.72 ± 0.74
	(-):	93.48	81.58	96.77
Fourier 2	P:	68.35	73.85	81.13
	(!):	24.07	25.00	39.53
		15.62 ± 15.37	8.11 ± 5.59	12.88 ± 11.64
	(-):	14.81	2.08	0.00
Fourier 3	P:	96.20	89.23	79.25
	(!):	11.84	13.79	19.05
		46.07 ± 30.56	18.66 ± 13.57	21.96 ± 18.31
	(-):	54.67	28.07	4.88
Fourier 4	P:	93.67	92.31	84.91
	(!):	16.22	23.33	15.56
		42.69 ± 25.75	21.08 ± 23.11	10.29 ± 9.71
	(-):	75.68	46.67	28.89

Table 13

		2%	3%
Closest curve method	MAPE ± SD (%)	19.05 ± 14.82	14.40 ± 8.40
	RMSE (%)	0.85	0.75
N closest curves method	MAPE ± SD (%)	15.44 ± 11.71	14.85 ± 11.81
	RMSE (%)	0.68	0.86

Table 14

		2%	3%
Closest curve method	MAPE ± SD (%)	14.43 ± 10.41	19.16 ± 14.31
	RMSE (%)	20.30	23.81
N closest curves method	MAPE ± SD (%)	12.67 ± 8.02	11.22 ± 7.27
	RMSE (%)	18.29	15.34

C.3.3 *Shape-based comparison method*

Table 12

	5%		6%		7%	
	C	NC	C	NC	C	NC
MAPE ± SD (%)	14.39 ± 11.26	9.96 ± 9.99	13.45 ± 10.6	10.21 ± 8.73	12.33 ± 9.6	8.14 ± 6.44
RMSE (%)	1.40	1.03	1.38	1.05	1.39	0.95
Percentage of overpredictions (%)	45.57	44.3	44.62	33.85	49.06	32.07
MAPE ± SD (%) of overpredictions	13.85 ± 12.42	13.10 ± 12.3	14.05 ± 11.53	14.60 ± 11.47	12.64 ± 9.30	6.96 ± 6.20

C.3.4 *Interspecies application*

Table 15

		2%	3%
Closest curve method	MAPE ± SD (%)	18.5 ± 10.8	10.53 ± 7.6
	RMSE (%)	11.55	6.72
N closest curves method	MAPE ± SD (%)	13.83 ± 9.58	10.91 ± 9.25
	RMSE (%)	7.7	6.93

REFERENCES

LC Almekinders and JD Temple. Etiology, diagnosis, and treatment of tendonitis: an analysis of the literature. *Medicine and science in sports and exercise*, 30(8):1183–1190, 1998. URL http://ukpmc.ac.uk/abstract/MED/9710855. 1

Gustav Andersson and PhD M D Patrik Danielson. *Influences of paratendinous innervation and non-neuronal substance P in tendinopathy*. PhD thesis, Umeå, Sweden, 2010. 1

Rausing A Aström M. Chronic Achilles tendinopathy. A survey of surgical and histopathologic findings. *Clin Orthop Relat Res.*, 316:151–164, 1995. 1

RAE Clayton. The epidemiology of musculoskeletal tendinous and ligamentous injuries. *Injury*, 39(12):1338–1344, 2008. URL http://www.sciencedirect.com/science/article/pii/S0020138308002982. 1

AC Devkota. *An in-vitro explant model of overuse tendinopathy. The effects of cyclic loading and inflammatory mediators on mechanical and compositional properties of tendons*, volume Doctor of. University of North Carolina, Chapel Hill, 2007. URL http://gradworks.umi.com/32/39/3239284.html. 1

BA Dowling and AJ Dart. Mechanical and functional properties of the equine superficial digital flexor tendon. *The Veterinary Journal*, 170(2):184–192, 2005. URL http://www.ncbi.nlm.nih.gov/pubmed/16129339http://www.sciencedirect.com/science/article/pii/S1090023304000838. 1

J Dudhia, CM Scott, and ERC Draper. Aging enhances a mechanically induced reduction in tendon strength by an active process involving matrix metalloproteinase activity. *Aging Cell*, 6:547–556, 2007. URL http://onlinelibrary.wiley.com/doi/10.1111/j.1474-9726.2007.00307.x/full. 1

J Flick, A Devkota, M Tsuzaki, L Almekinders, and P Weinhold. Cyclic loading alters biomechanical properties and secretion of PGE2 and NO from tendon explants. *Clin Biomech (Bristol, Avon)*, 21 (1):99–106, 2006. URL http://www.ncbi.nlm.nih.gov/pubmed/16198031. 1

DT Fung and VM Wang. Early response to tendon fatigue damage accumulation in a novel in vivo model. *Journal of Biomechanics*, 43(2):274–279, 2010. URL http://www.ncbi.nlm.nih.gov/pubmed/19939387http://www.sciencedirect.com/science/article/pii/S0021929009005375. 1

PhD Graham Riley. Tendinopathy – From Basic Science to Treatment: Molecular Composition of Tendon. *Nat Clin Pract Rheumatol.*, 4(2):82–89, 2008. 1

B. Sun Hui, Li Yonghui, T. Fung David, Y. Lee Jonathan, M. Wang Vincent, Basta-Pljakic Jelena, J. Leong Daniel, J. Ros Stephen, A. Klug Raymond, Braman Jonathan, B. Schaffler Mitch, J. Jepsen Karl, L. Flatow Evan, and Nelly Andarawis-Puri. Cycle-Dependent Matrix Remodeling Gene Expression Response in Fatigue-Loaded Rat Patellar Tendons. *Journal of Orthopaedic Research*, 2010. 1

H J Jung, M B Fisher, and S L Woo. Role of biomechanics in the understanding of normal, injured, and healing ligaments and tendons. *Sports Med Arthrosc Rehabil Ther Technol*, 1(1):9, 2009. URL http://www.ncbi.nlm.nih.gov/pubmed/19457264. 1

RF Ker, XT Wang, and AV Pike. Fatigue quality of mammalian tendons. *Journal of Experimental Biology*, 203:1317–1327, 2000. URL http://jeb.biologists.org/content/203/8/1317.short. 1

M Kongsgaard and P Aagaard. Structural Achilles tendon properties in athletes subjected to different exercise modes and in Achilles tendon rupture patients. *Journal of Applied . . .* , 99:1965–1971, 2005. URL http://jap.physiology.org/content/99/5/1965.short. 1

DPM* Matthew B. Werd. Achilles Tendon Injuries in Sports. A Review of Classification and Treatment. *J Am Podiatr Med Assoc*, 97:37–48, 2007. 1

Weinong Chen Ming Cheng and Tusit Weerasooriya. Mechanical Behavior of Bovine Tendon with Stress-Softening and Loading-Rate effects. *Advances in Theoretical and Applied Mechanics*, 2(2): 59–74, 2009. 4.1.1

Gad A Movin T Reinholt FP, Rolf C. Tendon pathology in long-standing achillodynia. Biopsy findings in 40 patients . *Acta Orthop Scand.*, 68(2):170–1 75, 1997. 1

LH Nakama and KB King. Evidence of tendon microtears due to cyclical loading in an in vivo tendinopathy model. *Journal of Orthopaedic Research*, 23(5):1199–1205, 2005. URL http://www.ncbi.nlm.nih.gov/pubmed/16140201http://onlinelibrary.wiley.com/doi/10.1016/j.orthres.2005.03.006/abstract. 1

M D Pekka Kannus PhD, László Józsa, M.D., PhD. Histopathological Changes Preceding Spontaneous Rupture of a Tendon . *The Journal of Bone and Joint Surgery*, 73-A:1507–1525, 1991. 1

AV Pike, RF Ker, and RM Alexander. The development of fatigue quality in high-and low-stressed tendons of sheep (Ovis aries). *Journal of Experimental Biology*, 203:2187–2193, 2000. URL http://jeb.biologists.org/content/203/14/2187.short. 1

J D Rees, A M Wilson, and R L Wolman. Current concepts in the management of tendon disorders. *Rheumatology (Oxford)*, 45(5):508–521, 2006a. URL http://www.ncbi.nlm.nih.gov/pubmed/16490749. 1

J D Rees, A M Wilson, and R L Wolman. Current concepts in the management of tendon disorders. *Rheumatology (Oxford, England)*, 45(5):508–21, May 2006b. ISSN 1462-0324. URL http://rheumatology.oxfordjournals.org/cgi/content/long/45/5/508. 1

G Riley. The pathogenesis of tendinopathy. A molecular perspective. *Rheumatology (Oxford)*, 43(2): 131–142, 2004. URL http://www.ncbi.nlm.nih.gov/pubmed/12867575. 1

AA Schepsis, H Jones, and AL Haas. Achilles tendon disorders in athletes. *The American Journal of Sports Medicine*, 30:287–305, 2002. URL http://ajs.sagepub.com/content/30/2/287.short. 1

M Shannon. Lower limb biomechanics during running in individuals with Achilles tendinopathy: a systematic review. *Journal of Foot and Ankle Research*, 4:15, 2011. URL http://www.ncbi.nlm.nih.gov/pubmed/21619710http://www.doaj.org/doaj?func=abstract&id=797168. 1

P Sharma and N Maffulli. Tendon injury and tendinopathy: healing and repair. *The Journal of Bone & Joint Surgery*, 87(1):187–202, 2005. URL http://www.ncbi.nlm.nih.gov/pubmed/15634833http://jbjs.org/article.aspx?Volume=87&page=187. 1

GM Thornton and DA Hart. The interface of mechanical loading and biological variables as they pertain to the development of tendinosis. *J Musculoskelet Neuronal Interact*, 11:94–105, 2011. URL http://www.ismni.org/jmni/pdf/44/03THORNTON.pdf. 1

C T Thorpe, R J Stark, A E Goodship, and H L Birch. Mechanical properties of the equine superficial digital flexor tendon relate to specific collagen cross-link levels. *Equine Vet J*, 42 Suppl 3:538–543, 2010. URL http://www.ncbi.nlm.nih.gov/pubmed/21059057. 1

M De Zee, F Bojsen-Mø ller, and M Voigt. Dynamic viscoelastic behavior of lower extremity tendons during simulated running. *Journal of Applied Physiology*, 89:1352–1359, 2000. URL http://www.jappl.org/content/89/4/1352.short. 1